# SCATTERING OF LASER LIGHT BY LABORATORY PLASMAS

by

PING WAH CHAN

B.Sc., University of Hong Kong, 1962

M.Sc., University of British Columbia, 1964

A THESIS SUBMITTED IN PARTIAL FULFILMENT OF

THE REQUIREMENTS FOR THE DEGREE OF

DOCTOR OF PHILOSOPHY

in the Department

of

PHYSICS

We accept this thesis as conforming to the

required standard

THE UNIVERSITY OF BRITISH COLUMBIA

May, 1966

In presenting this thesis in partial fulfilment of the requirements for an advanced degree at the University of British Columbia, I agree that the Library shall make it freely available for reference and study. I further agree that permission for extensive copying of this thesis for scholarly purposes may be granted by the Head of my Department or by his representatives. It is understood that copying or publication of this thesis for financial gain shall not be allowed without my written permission.

Department of Physics

The University of British Columbia
Vancouver 8, Canada

Date June 17, 1966

The University of British Columbia

FACULTY OF GRADUATE STUDIES

PROGRAMME OF THE

FINAL ORAL EXAMINATION

FOR THE DEGREE OF

DOCTOR OF PHILOSOPHY

of

PING WAH CHAN

B.Sc., The University of Hong Kong, 1962

M.Sc., The University of British Columbia, 1964

IN ROOM 301, HENNINGS BUILDING

FRIDAY, JUNE 17, 1966, AT 10:30 A.M.

COMMITTEE IN CHARGE

Chairman: L. D. Hayward

B. Ahlborn
A. J. Barnard
A. M. Crooker
F. L. Curzon
M. M. Z. Kharadly
R. A. Nodwell

External Examiner: S. A. Ramsden

National Research Coundil

Ottawa

Research Supervisor: R. A. Nodwell

# SCATTERING OF LASER LIGHT BY LABORATORY PLASMAS


## ABSTRACT

The scattering of laser light by laboratory plasmas has been observed. When the scattering was from a plasma formed in a θ-pinch, with scattering angle of 90°, a nearly Gaussian profile of the scattered intensity as a function of wavelengths was observed, corresponding to scattering by non-interacting electrons. When the scattering was from a plasma jet, with scattering angle of 45° from the forward direction, distinct satellite peaks were observed on both sides of a narrow central peak at the laser frequency as predicted by theory,[1,2,3,4] indicating a strong collective scattering effect between the electrons and the ions. The widths of the satellite lines were greater than the values predicted by theory. The discrepancy is ascribed to spatial variations in the electron density in the volume of the observed plasma. The intensities and frequencies at which they occur these peaks also vary with the current of the plasma jet in a manner consistent with theory. The scattered intensity of the central peak was measured approximately and it agrees with theoretical prediction. Some indication of perturbation of the plasma by the incident laser light has also been observed.



1. E.E. Salpeter, Phys. Rev. 120, 1528(1960).
2. J.A. Fejer, Can. J. Phys. 38, 1114(1960).
3. J.P. Dougherty and D.T. Farley, Pro. Roy. Soc. (London) A259, 79(1960).
4. M.N. Rosenbluth and N. Rostoker, Phys. Fluids 5, 776(1962).

# GRADUATE STUDIES

Field of Study: Physics

| | |
|---|---|
| Elementary Quantum Mechanics | W. Opechowski |
| Waves | J. Savage |
| Electromagnetic Theory | G. M. Volkoff |
| Plasma Physics | L. Sobrino |
| Special Relativity | H. Schmidt |
| Spectroscopy | A. M. Crooker<br>A. J. Barnard |
| Advanced Plasma Physics | A. J. Barnard |
| Plasma Dynamics | F. L. Curzon |

## PUBLICATION

Collective Scattering of Laser Light by a Plasma-

P. W. Chan & R. A. Nodwell

Phys. Rev. Letters 16, 122 (1966).

PING WAH CHAN. SCATTERING OF LASER LIGHT BY LABORATORY PLASMAS.
Supervisor: Dr. R. A. Nodwell.

## ABSTRACT

The scattering of laser light by laboratory plasmas has been observed. When the scattering was from a plasma formed in a θ- pinch, with scattering angle of $90^{o}$, a nearly Gaussian profile of the scattered intensity as a function of wavelength was observed, corresponding to scattering by non-interacting electrons. When the scattering was from a plasma jet, with scattering angle of $45^{o}$ from the forward direction, distinct satellite peaks were observed on both sides of a narrow central peak at the laser frequency as predicted by theory,[1,2,3,4] indicating a strong collective scattering effect between the electrons and the ions. The widths of the satellite lines were greater than the values predicted by theory. The discrepancy is ascribed to spatial variations in the electron density in the volume of the observed plasma. The intensities of the peaks and frequencies at which they occur also vary with the current of the plasma jet in a manner consistent with theory. The scattered intensity of the central peak was measured approximately and it agrees with theoretical prediction. Some indication of perturbation of the plasma by the incident laser light has also been observed.

## TABLE OF CONTENTS

# FIGURE CAPTIONS

## ACKNOWLEDGEMENT

I wish to thank Dr. R.A. Nodwell for his invaluable supervision and encouragement during the whole course of this work.

Thanks are also due to Dr. J.H. Williamson for his service in programming the theoretical curves and best fits, to Dr. B. Ahlborn and Mr. R. Morris for their assistance in setting up the plasma jet, to Dr. L. de Sobrino for his help in the theoretical aspects of this work, and to Dr. J.A. Barnard, Dr. A.M. Crooker, Dr. F.L. Curzon for reading and improving this thesis.

The assistance of Mr. W. Ratzlaff and Mr. J. Dooyeweerd in the work of electronics, and the assistance of Mr. J. Lees and Mr. T. Knopp in the construction of the apparatus is deeply appreciated.

Financial assistance in the form of a NRC Studentship during the course of this work is also gratefully acknowledged.

This work is supported by a grant of the Atomic Energy Control Board of Canada.

## CHAPTER I INTRODUCTION

In recent years there has been a very great increase in interest in the properties of electromagnetic radiation scattered by a plasma. This interest was stimulated by an observation made by Bowles,[5] who found that the spectral profile of the back scattered radiation from a radar beam incident on the ionosphere has a very narrow width corresponding to Doppler broadening due to the ion velocity. Following the publication of these results, the theory of scattering of electromagnetic waves by a plasma has been developed by Salpeter,[1] Fejer,[2] Dougherty and Farley,[3] and Rosenbluth and Rostoker.[4] This theory predicts that, if the wavelength of the incident radiation is large compared with the Debye length of the plasma, the scattered profile consists of a central peak and two weak satellite lines at approximately the plasma frequency from the central frequency. Recently Perkins, Salpeter and Yngnessen,[6] have observed these satellite lines scattered by the ionosphere using a very powerful radar beam. Stern and Tzoar,[7] have also observed the satellite lines by enhancing the longitudinal electrostatic oscillations in the plasma with microwaves.

Because of the success of the theory in explaining Bowle's results and the possibility of determining interesting plasma parameters such as electron and ion temperature; electron density at a small point in space and time, it is natural that plasma physicists everywhere have been intrigued with the possibility of using scattering of radiation as a diagnostic tool in laboratory plasmas. It has been found difficult, however, to apply the

technique to laboratory plasmas mainly because of the extremely small scattering cross section for electrons. It is only with the recent development of lasers which are very powerful monochromatic light sources that experiments of this kind in the laboratory have become feasible. The first successful laboratory experiment was reported by Fiocco and Thompson,[8] who scattered laser light from an electron beam. Subsequently several workers have used this technique for diagnosis of plasma properties. Funfer, Kronast, and Kunze and Kegel,[9,10]; and Davies and Ramsden,[11] have reported scattering of light from a theta pinch and have obtained a nearby Gaussian scattered profile corresponding to scattering by non-interacting electrons. However, until very recently the numerous attempts to observe the satellite lines have not been successful. The chief difficulties have been the problem of eliminating the stray light from walls, windows and impurities and the problem of obtaining a uniform and constant plasma. Several reports have been made,[12,13,14,] in which there is an indication that a satellite may be present but the results are ambiguous. Two papers have appeared in the literature recently in which the unambiguous observation of satellites in laboratory experiments are reported. Ramsden and Davies,[15] report observing the satellites using a theta pinch device. The plasma source employed by the author (Chan and Nodwell)[16] is a plasma jet.

In this thesis we wish to report on the observations made on the profiles of the scattered radiation from plasmas formed in the theta pinch and also in a high current d.c. plasma jet. Chapter 2 is a summary of the theory of the scattering in which

the physical significance of the steps in the derivations are discussed and a resumé of the assumptions and the results is given, For those readers interested in a more detailed theoretical discussion a more complete derivation is given in the Appendix. In Chapter 3 we discuss the practical difficulties in the design of a scattering experiment and give possible experimental techniques to overcome these difficulties. Chapter 4 is devoted to a particular discussion of the scattering from a theta pinch plasma and Chapter 5 describes the experiment on the plasma jet. The last chapter (Chapter 6) summarizes the results obtained and discusses the significance of these results. The advantages and disadvantages of the scattering method as a diagnostic tool are discussed and suggestions for future work given.

## CHAPTER II THEORY

The power flux spectrum of electromagnetic waves scattered by electrons in a plasma will first be calculated in section A using the Thomson theory. We shall see that this expression contains a term involving the calculation of the ensemble average of the Fourier transform of the electron density. This quantity has been calculated by Salpeter,[1] Fejer,[2] Dougherty and Farley,[3] and Rosenbluth and Rostoker.[4] In calculating this quantity, we use a method of superposition of dressed test particles suggested by Rosenbluth and Rostoker.[4] (A dressed test particle is a charged particle in which the screening strength of the surrounding plasma is allowed for by postulating an attendant polarization cloud). The detailed mathematical derivations are given in the Appendix, and only the assumptions and principal predictions of this calculation are included here in section B. A graphical presentation and a discussion of these results are given in section C.

### (A) Thomson Scattering from Electrons in a Plasma

Fig. 1 shows the geometry of scattering of electromagnetic wave by a plasma. Consider a charge with velocity $\underline{v}$ under the influence of a plane electromagnetic wave of frequency $\Omega_i$, and wave vector $\underline{K}_i$. Assume that the incremental velocity produced on the charge by the field $\underline{E}$ is negligible compared with the velocity $\underline{v}$ and that $v/c \ll 1$ where c is the velocity of light, that is we consider a non-relativistic plasma not heated by the incident wave. Quantum-mechanical effects are also neglected. Since only a very small part of the incident radiation is scattered, so that we can use the first Born approximation and

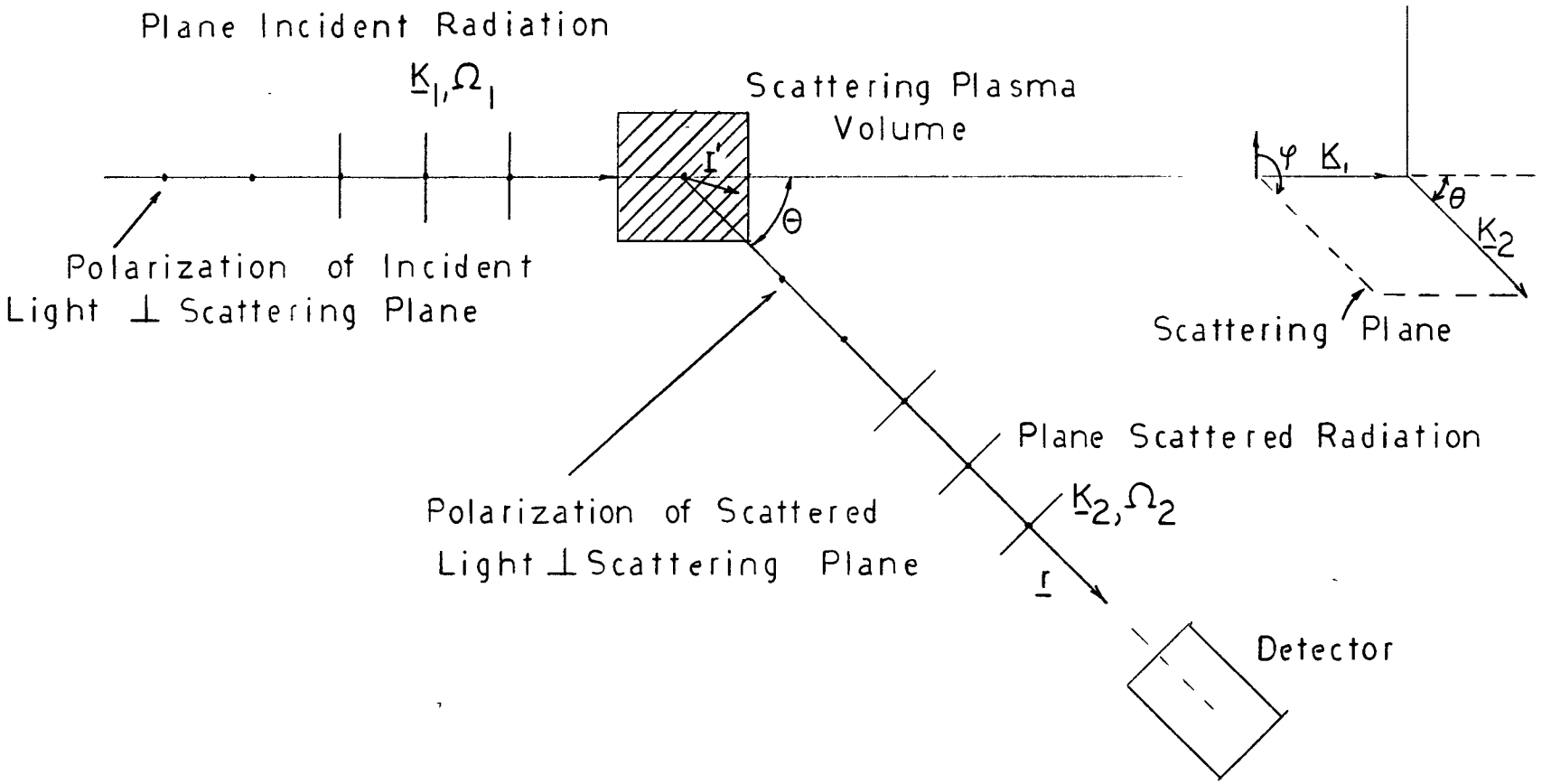


**Fig. 1: Geometry of Scattering of Electromagnetic Radiation by a Plasma**

write the total field at $\underline{r}'$ as the incident field.

$$\underline{E} = \underline{E}_o \exp\left[-i(\Omega_i t - \underline{k}_i \cdot \underline{r}')\right] \tag{1}$$

The acceleration of an electron particle at $\underline{r}'$ under the influence of the plane wave is

$$\dot{\underline{v}} = \frac{q_e}{m_e} \underline{E}_o \exp\left[-i(\Omega_i t' - \underline{k}_i \cdot \underline{r}')\right] \tag{2}$$

where $q_e$, $m_e$, are the charge and mass of the electron respectively. (Scattering due to ions can be neglected because of their heavy mass) The radiation field of a single accelerated electron at an observation point $\underline{r}$ at time t is given by

$$\underline{E}_{rad} = \frac{e}{c^2} \frac{\underline{r} \times (\underline{r} \times \dot{\underline{v}}(t'))}{r^3} = r_o \frac{\underline{r} \times (\underline{r} \times \underline{E}_o)}{r^3} \exp\left[-i(\Omega_i t' - \underline{k}_i \cdot \underline{r}')\right] \tag{3}$$

where $e^2/mc^2 = r_o$ = classical electron radius

$$t' \simeq t - \frac{r}{c} + \frac{\underline{r}' \cdot \hat{r}}{c} \qquad (\because r \gg r')$$

$\hat{r}$ is a unit vector in the direction of $\underline{r}$.

The total field $\underline{E}_s$ scattered by the electron distribution $n_e(\underline{r},t)$ is the vector sum of the contribution from individual electrons and is given by

$$\underline{E}_s(t) = r_o \frac{\underline{r} \times (\underline{r} \times \underline{E}_o)}{r^3} \int d\underline{r}' \, n_e(\underline{r}', t') \exp\left[-i(\Omega_i t' - \underline{k}_i \cdot \underline{r}')\right] \tag{4}$$

where

$$n_e(\underline{r}, t) = \sum_j \delta(\underline{r} - \underline{r}_j(t)) \tag{5}$$

where $\underline{r}_j$ is the position of the $j^{th}$ electron

At the point of observation the scattered wave may be considered plane, so that the magnitude of the scattered power flux is

$$S(t) = \frac{c}{4\pi} E_s^2(t) \tag{6}$$

To convert this time function of flux to a frequency function of flux we take the Fourier transform and apply Parseval's

Theorem[17]

$$S(\Omega_2) = \frac{c}{8\pi^2} \left| \tilde{\underline{E}}_s(\Omega_2) \right|^2 \tag{7}$$

where

$$\tilde{\underline{E}}_s(\Omega_2) = \int_{-\infty}^{\infty} e^{i\Omega_2 t} \underline{E}_s(t)\, dt \tag{8}$$

is the Fourier transform of $\underline{E}_s(t)$.

Combining equation (4) and (8) and expressing t in terms of t', we get

$$\begin{aligned} \tilde{\underline{E}}_s(\Omega_2) &= \underline{\mathcal{E}} \int_{-\infty}^{\infty} dt' \int d\underline{r}'\, e^{i\Omega_2 (t' + \frac{r}{c} - \frac{\underline{r}'\cdot\hat{r}}{c})} n_e(\underline{r}', t')\, e^{-i(\Omega_1 t - \underline{k}_1 \cdot \underline{r}')} \\ &= \underline{\mathcal{E}}\, e^{i\Omega_2 r/c} \int d\underline{r}'\, e^{-i(\frac{\Omega_2}{c}\hat{r} - \underline{k}_1)\cdot \underline{r}'} \tilde{n}_e(\underline{r}', \Omega_2 - \Omega_1) \end{aligned} \tag{9}$$

or

$$\tilde{\underline{E}}_s(\Omega_2) = \underline{\mathcal{E}}\, e^{i\Omega_2 r/c}\, \hat{\tilde{n}}_e\left(\Omega_2 \frac{\hat{r}}{c} - \underline{k}_1 , \Omega_2 - \Omega_1\right) \tag{10}$$

where

$$\underline{\mathcal{E}} \equiv \frac{r_0}{r^3}\, \underline{r} \times (\underline{r} \times \underline{E}_0) \tag{11}$$

$$\tilde{n}_e(\underline{r}', \Omega_2 - \Omega_1) \equiv \int dt'\, e^{i(\Omega_2 - \Omega_1)t'} n_e(\underline{r}', t') \tag{12}$$

$$\hat{\tilde{n}}_e\left(\Omega_2 \frac{\hat{r}}{c} - \underline{k}_1 , \Omega_2 - \Omega_1\right) \equiv \int d\underline{r}'\, e^{-i(\frac{\Omega_2}{c}\hat{r} - \underline{k}_1)\cdot \underline{r}'} \tilde{n}_e(\underline{r}', \Omega_2 - \Omega_1) \tag{13}$$

The power spectrum density is therefore given by

$$S(\Omega_2) = \frac{c\, \mathcal{E}^2}{8\pi^2} \left| \hat{\tilde{n}}_e\left(\Omega_2 \frac{\hat{r}}{c} - \underline{k}_1 , \Omega_2 - \Omega_1\right) \right|^2 \tag{14}$$

Because the observation time is long compared with the fluctuation time, we are interested in the ensemble average of this quantity, i.e.

$$\left\langle S(\Omega_2) = \frac{c\, \mathcal{E}^2}{8\pi^2} \left\langle \left| \hat{\tilde{n}}_e\left(\Omega_2 \frac{\hat{r}}{c} - \underline{k}_1 , \Omega_2 - \Omega_1\right) \right|^2 \right\rangle \right. \tag{15}$$

Finally the scattered power spectrum density may be written as

$$\langle S(\omega) \rangle = N \frac{c}{4\pi} E_0^2 \frac{r_0^2}{r^2} (1 - \sin^2\theta \cos^2\varphi) \langle |\hat{\tilde{n}}_e(k, \omega)|^2 \rangle \tag{16}$$

where

N is the total number of scattering electrons,

$\theta$ is the scattering angle (see Fig. 1)

$\varphi$ the angle between the electric vector $\underline{E}$ of the incident light (assumed to be linearly polarized) and the scattering plane defined by $\underline{K}_1$ and $\underline{K}_2 = \frac{\Omega_2}{c}\hat{r}$ and

$\underline{k} = \underline{K}_1 - \underline{K}_2$

$\omega = \Omega_1 - \Omega_2$

(B) Calculation of $\langle |\hat{n}_e(k,\omega)|^2 \rangle$

Consider a plasma with average electron density $n_o$, electron temperature $T_e$ and ion temperature $T_i$ and electron Debye length $\lambda_D = \left(\frac{kT_e}{4\pi n_o e^2}\right)^{1/2}$ where $e$ is the electron charge and $k$ the Boltzmann constant. The following assumptions are made:

(i) The electrons and ions have Maxwellian velocity distributions, but $T_e$ is not necessarily equal to $T_i$.

(ii) There is no external magnetic field.

(iii) There is no electron drift relative to the ions.

(iv) We assume that a sphere of radius equal to the Debye length contains many electrons, i.e. the quantity

$$\Lambda = n_o \lambda_D^3 \simeq \frac{\lambda_D k T_e}{e^2} \gg 1 \qquad (17)$$

The inquality implies that the Coulomb interaction $(e^2/\lambda_D)$ between nearby electrons is small compared to the thermal kinetic energy $kT_e$.

(v) We further assume that the scaling length $\underline{k}$ defined as $k \equiv 4\pi\lambda^{-1}\sin(\theta/2)$ where $\lambda$ is the incident wavelength and $\theta$ is the scattering angle from the forward direction is small compared with the small-angle Coulomb and electron-neutral mean free paths so that collisions may be neglected in the calculation.[18]

The plasma is considered to consist of fully dressed test particles that are uncorrelated, that is that the test particles move with assigned orbits through the plasma with particle distribution function described by the Vlasov equations. We also assume that the variation of the particle distribution function is negligible during times of the order of $\omega_p^{-1}$ and that the spatial inhomogeneity is negligible over distance of the order of the Debye length ($\lambda_D$). More general cases have been considered by Rosenbluth and Rostoker[4] including the calculation in the presence of a constant magnetic field and the case when there is an electron drift relative to the ions.

The quantity $\frac{\langle|\hat{n}_e(k,\omega)|^2\rangle}{n_0}$ is the double Fourier transform of the density autocorrelation function defined as

$$C(\rho,\tau) \equiv \frac{\langle n_e(\underline{r},t)\, n_e(\underline{r}+\underline{\rho},\, t+\tau)\rangle}{n_0} \tag{18}$$

as can be seen,

$$\begin{aligned} &\int_{-\infty}^{\infty} d\tau\, e^{i\omega\tau} \int_{-\infty}^{\infty} d\underline{\rho}\, e^{-i\underline{k}\cdot\underline{\rho}} \left\langle \int d\underline{r} \int dt\, \frac{n_e(\underline{r},t)\, n_e(\underline{r}+\underline{\rho},\, t+\tau)}{n_0} \right\rangle \\ &= \frac{1}{n_0} \left\langle \iint_{-\infty}^{+\infty} dt\, dt'\, e^{i\omega(t'-t)} \iint d\underline{r}'\, d\underline{r}\, e^{-i\underline{k}\cdot(\underline{r}'-\underline{r})}\, n_e(\underline{r},t)\, n_e(\underline{r}',t') \right\rangle, \quad \left.\begin{matrix} t+\tau = t' \\ \underline{r}+\underline{\rho} = \underline{r}' \end{matrix}\right\} \\ &= \frac{1}{n_0} \langle \hat{n}_e(\underline{k},\omega)\, \hat{n}_e(-\underline{k},-\omega)\rangle = \frac{1}{n_0} \langle |\hat{n}_e(k,\omega)|^2 \rangle \end{aligned} \tag{19}$$

It turns out that it is easier to calculate the quantity $C(\rho,\tau)$ and get the quantity $\langle|\hat{n}_e(k,\omega)|^2\rangle$ by subsequent double transform. This is sufficient for a stationary spatially homogeneous plasma (which we have assumed) because the density autocorrelation function is independent of $\underline{r}$ and t and the statistical averaging can be interchanged with the $\underline{r}$ and t integrations.

The method of superpositions of dressed test particles consists in finding the effect on the number density due to a test particle at a given position with a given velocity. By assuming the test particles to be uncorrelated, the statistical average is

calculated by integrating over the volume of the plasma and over all velocities for all species of the particles. This calculation is carried out in the Appendix and the final results, given in Salpeter's form, is

$$\langle |\hat{n}_e(k,\omega)|^2 \rangle = \frac{2\pi}{k} \frac{|1-G_i|^2 F_e(u) + Z|G_e|^2 F_i(u)}{|1-G_e-G_i|^2} \tag{20}$$

where $Z$ = degree of ionization

$$F_e(u) = \left(\frac{m_e}{2\pi kT_e}\right)^{\frac{1}{2}} e^{-m_e u^2/2kT_e}$$

$$F_i(u) = \left(\frac{m_i}{2\pi kT_i}\right)^{\frac{1}{2}} e^{-m_i u^2/2kT_i}$$

$$G_e(\omega) = -\alpha^2[1-f(x)+i\pi^{\frac{1}{2}}x\exp(-x^2)]; \quad x=\frac{\omega}{\omega_e}, \quad \omega_e=\left(\frac{2k^2kT_e}{m_e}\right)^{\frac{1}{2}}$$

$$G_i(\omega) = -\frac{ZT_e\alpha^2}{T_i}[1-f(y)+i\pi^{\frac{1}{2}}y\exp(-y^2)]; \quad y=\frac{\omega}{\omega_i}, \quad \omega_i=\left(\frac{2k^2kT_i}{m_i}\right)^{\frac{1}{2}}$$

$$f(x) = 2x\exp(-x^2)\int_0^x \exp t^2\,dt$$

$$\alpha = \frac{1}{k\lambda_D} = \left(\frac{4\pi n_0 e^2}{k^2 kT_e}\right)^{\frac{1}{2}} = \lambda\left(\frac{n_0 e^2}{4\pi kT_e}\right)^{\frac{1}{2}} \frac{1}{\sin(\theta/2)}$$

where $\lambda$ is the wavelength of incident radiation

## (C) Discussion of Theoretical Results

We consider the case of practical interest, that is with $m_e \ll m_i$ and $T_i \lesssim T_e$. It is shown in the Appendix that the general expression (20) can be reduced to

$$\langle |\hat{n}_e(k,\omega)|^2 \rangle d\omega = \frac{2\pi}{k}\left[\Gamma_\alpha(x)\frac{d\omega}{\omega_e} + Z\left(\frac{\alpha^2}{1+\alpha^2}\right)^2 \Gamma_\beta(y)\frac{d\omega}{\omega_i}\right] \tag{21}$$

where $\beta^2 = \dfrac{ZT_e\alpha^2}{T_i(1+\alpha^2)}$

$$\Gamma_\alpha(x) = \exp(-x^2)\{[1+\alpha^2-\alpha^2 f(x)]^2 + \pi\alpha^4 x^2 \exp(-2x^2)\}^{-1}$$

$$\Gamma_\beta(y) = \exp(-y^2)\{[1+\beta^2-\beta^2 f(y)]^2 + \pi\beta^4 y^2 \exp(-2y^2)\}^{-1}$$

The essential features of the scattered spectral density will be determined by the shape of the functions $\Gamma_\alpha(x)$ and $\Gamma_\beta(y)$, both being even functions of x and y respectively. The shapes of the functions $\Gamma_\alpha(x)$ has been given by Salpeter[1] for various values of $\alpha$. The parameter $\alpha = \frac{\lambda}{4\pi \lambda_D \sin(\theta/2)}$ is a measure of the ratio of incident radiation wavelength to the Debye length and controls the degree of collective scattering whereas $x = \omega\left(\frac{2k^2kT_e}{m_e}\right)^{-\frac{1}{2}}$ is a measure of frequency at which scattering is observed.

We shall consider the shapes of the scattered profile for several values of $\alpha$.

(i) $\alpha \ll 1$

Physically this corresponds roughly to the case when the wavelength of the incident radiation ($\lambda$) is smaller than the Debye length ($\lambda_D$) of the plasma. When $\lambda \ll \lambda_D$, the phases of the wavelets scattered by electrons within a Debye sphere is uncorrelated, and one therefore expect the scattered spectrum to be Doppler broadened by the random thermal electron velocity. Fig. 2 shows some theoretical curves of the scattered profile for $T_e = 25{,}000^\circ$ K for several small values of $\alpha$. As $\alpha$ tends to zero, $\Gamma_\alpha(x)$ becomes $\Gamma_0(x) = \exp(-x^2)$ and has a Gaussian shape with a spread characterised by the electron thermal velocity. The width of this spread at half intensity is by definition given by

$$x^2 \equiv \left(\frac{\omega}{\omega_e}\right)^2 = \ln 2 \tag{22}$$

or

$$\Delta\Omega = \omega - 2\frac{\Omega}{c}\sin\frac{\theta}{2}\left(\frac{2kT_e}{m_e}\ln 2\right)^{\frac{1}{2}} \tag{23}$$

In wavelength units (21) becomes

$$\Delta\lambda = 2\frac{\lambda}{c}\sin\frac{\theta}{2}\left(\frac{2kT_e}{m_e}\ln 2\right)^{\frac{1}{2}} \tag{24}$$

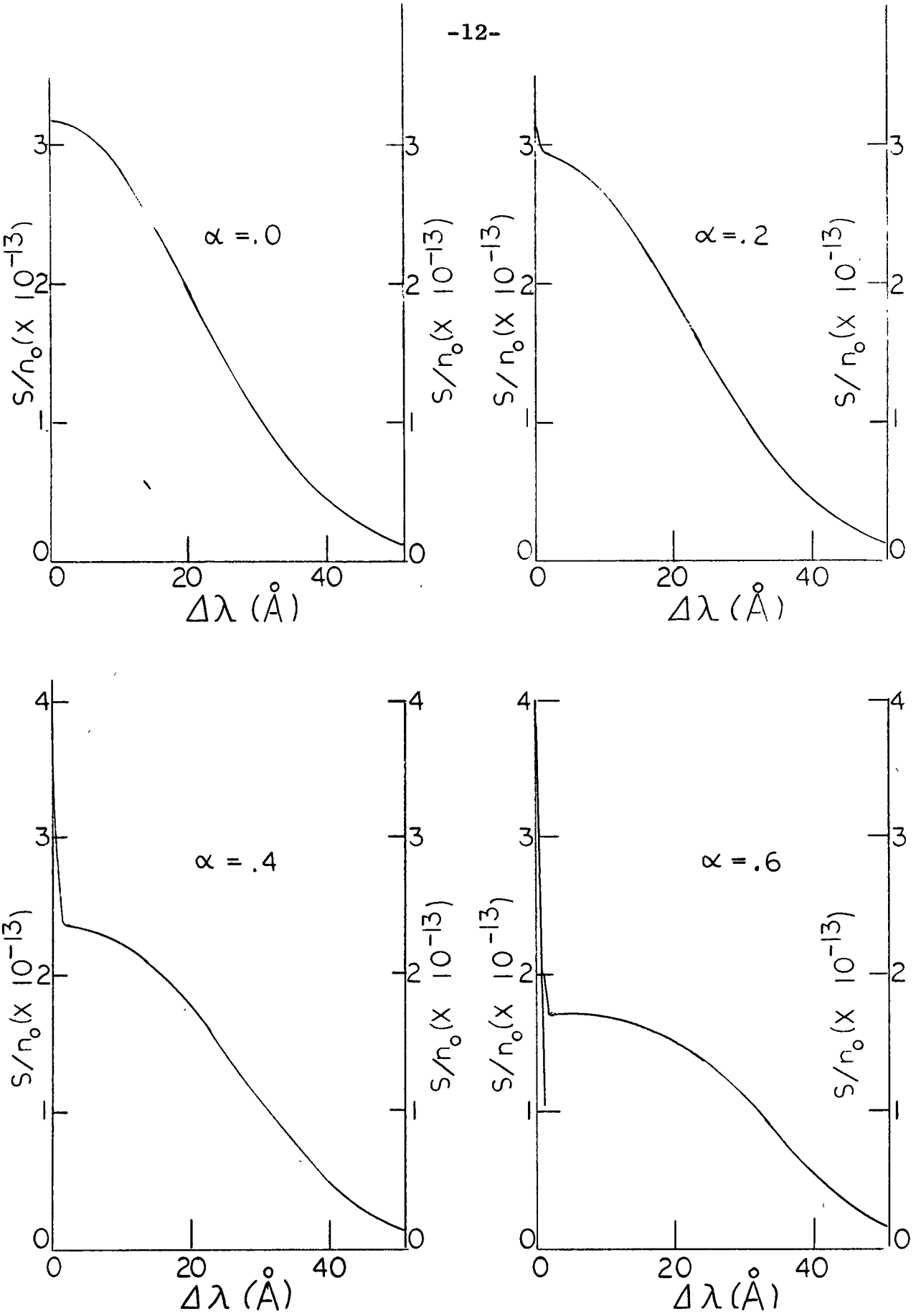


Fig. 2: Theoretical Scattered Spectrum for $\alpha < 1$ calculated for Hydrogen Plasma with $Z = 1$, $T_e = 25{,}000^{\circ}K$, $\theta = 90^{\circ}$

where the relation

$$\frac{\Delta\lambda}{\lambda} = -\frac{\Delta\Omega}{\Omega} \tag{25}$$

has been used.

The total width at half intensity (twice $\Delta\lambda$ ) is therefore

$$\Delta\lambda_{\frac{1}{2}} = 4\frac{\lambda}{c}\sin\frac{\theta}{2}\left(\frac{2k^2 kT_e}{m_e}\ln 2\right)^{\frac{1}{2}} \tag{26}$$

The contribution from the second term of (19), i.e. from $Z\left(\frac{\alpha^2}{1+\alpha^2}\right)^2 \Gamma_\beta(y)$ is negligible compared to the contribution from the first term $\Gamma_\alpha(x)$ because it is a factor $\alpha^4$ smaller. (Central peaks in Fig. 2)

(ii) $\alpha \sim 1$

Some typical scattered profiles for a $T_e = 25{,}000^{\circ}K$ are shown in Fig. 3 where we see that the electron satellite peaks begin to emerge as $\alpha$ approaches unity. The integrated intensities of the two contributions from $\Gamma_\alpha(x)$ and $\Gamma_\beta(y)$ can be obtained by direct integration (see Appendix) and one obtains

$$\pi^{-\frac{1}{2}}\int_{-\infty}^{\infty}\Gamma_\alpha(x)\,dx = \frac{1}{1+\alpha^2} \tag{27}$$

$$\pi^{-\frac{1}{2}}\left(\frac{\alpha^2}{1+\alpha^2}\right)^2\int_{-\infty}^{\infty}\Gamma_\beta(y)\,dy = \frac{1}{1+\alpha^2}\left(\frac{\alpha^4}{1+2\alpha^2}\right) \tag{28}$$

Therefore the total intensity is proportional to $\frac{1+\alpha^2}{1+2\alpha^2}$ . For small values of $\alpha$, this is unity and corresponds to the classical Thomson scattering cross-section. As $\alpha$ increases, this factor approaches to half asymptotically. The ratio of integrated intensity of each satellite to the central peak is 1/2 to $\frac{\alpha^4}{1+2\alpha^2}$ , and approaches $\alpha^{-2}$ for large $\alpha$.

(iii) $\alpha \gg 1$

In this case the wavelength of the incident radiation is larger than the Debye length and the electrons act collectively

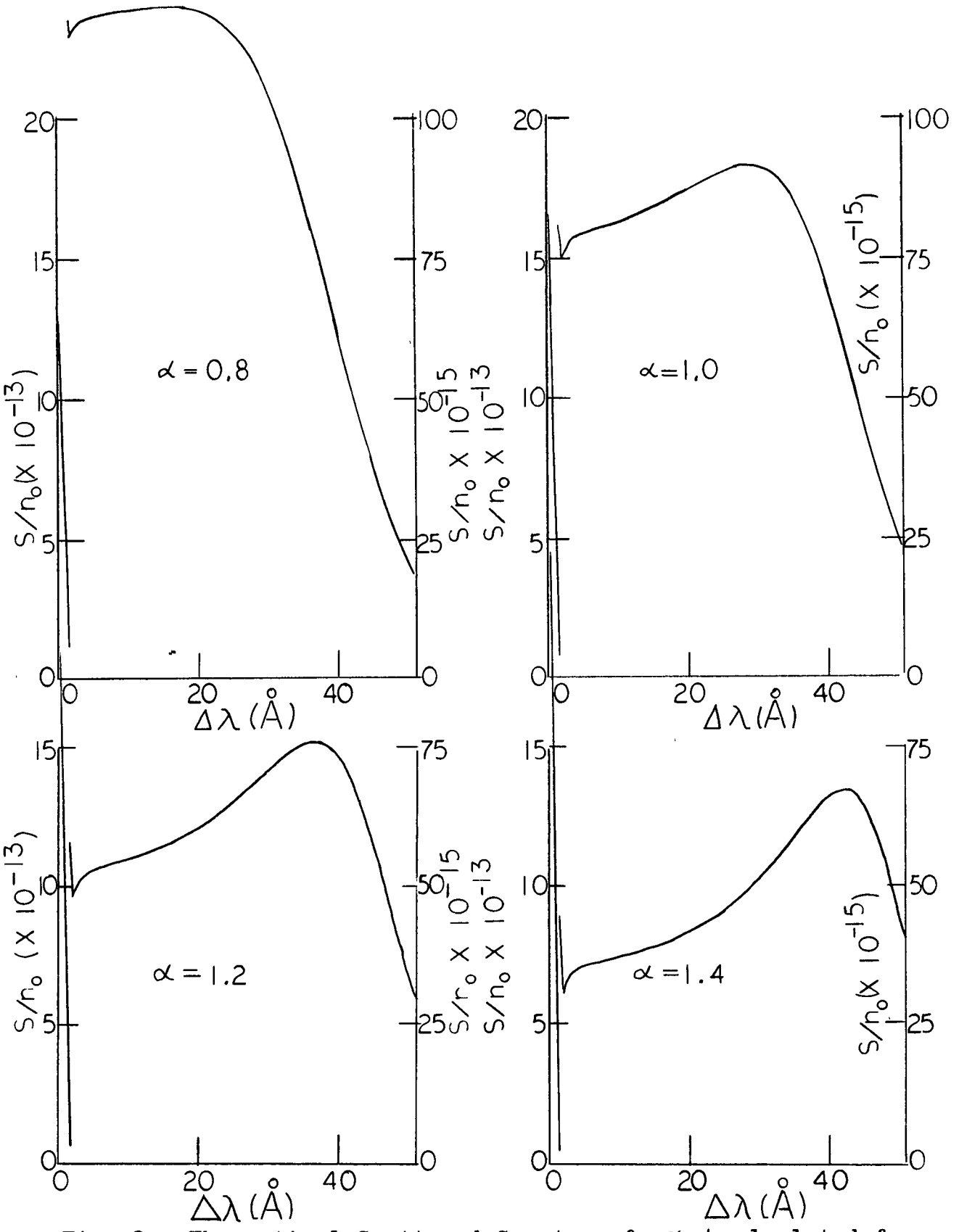


Fig. 3: Theoretical Scattered Spectrum for $\alpha \sim 1$ calculated for Hydrogen Plasma with Z = 1, $T_e = 25{,}000^{\circ}K$, $\theta = 90^{\circ}$

and scatter the incident radiation as a cloud.

It is shown in the Appendix that $\Gamma_\alpha(x)$ has a very sharp maximum near $x = \pm x_o$ where $x_o$ is the solution of

$$x_0^2 = \frac{1}{2}(\alpha^2+3) \tag{29}$$

or

$$\omega_0^2 = \omega_{pe}^2 + \frac{3k^2\kappa T_e}{m_e} \tag{30}$$

which is the well known dispersion relation for longitudinal electrostatic plasma oscillations.

In addition when x is very near $x_o$, $\Gamma_\alpha(x)$ can be approximated by the Lorentzian shape, (see Appendix)

$$\Gamma_\alpha(x) \simeq \frac{1}{2}\alpha^2 \exp(-x^2)\left\{4(x-x_0)^2 + \left[\tfrac{1}{2}\pi^{\frac{1}{2}}\alpha^4 \exp(-x_0^2)\right]^2\right\}^{-1} \tag{31}$$

The widths of these maxima are due to the so-called Landau damping of the plasma oscillations. The integrated intensity of each maximum is given by (see Appendix)

$$\pi^{-\frac{1}{2}} \int_0^\infty \Gamma_\alpha(x)\, dx = \frac{1}{2}\alpha^{-2} \tag{32}$$

and decreases rapidly as $\alpha$ increases although the height increases very rapidly. Fig. 4 shows some theoretical scattered profiles for several values of $\alpha > 1$ at a $T_e = 13{,}500^\circ K$. It should be remembered that although the theoretical widths of these "satellites" peaks are very narrow, in practice small variations of the electron density will vary the plasma frequency and will broaden the spectrum of these "satellites". Collision may also broaden these "satellites."

The contribution from the second term involving $\Gamma_\beta(y)$ is important only for small frequency shifts. The integrated intensity of this term gives the intensity of the 'central peak' of the scattered spectrum and varies as $\frac{\alpha^4}{(1+\alpha^2)(1+2\alpha^2)}$ (see Appendix). If $Z = \frac{T_i}{T_e} = 1$, $\beta = 1$ as $\alpha \to \infty$ and $\Gamma_\beta(y)$ has a flat-top shape. If $ZT_e > T_i$ as well as $\alpha \gg 1$, we have $\beta \gg 1$ and the ion component $\Gamma_\beta(y)$ has

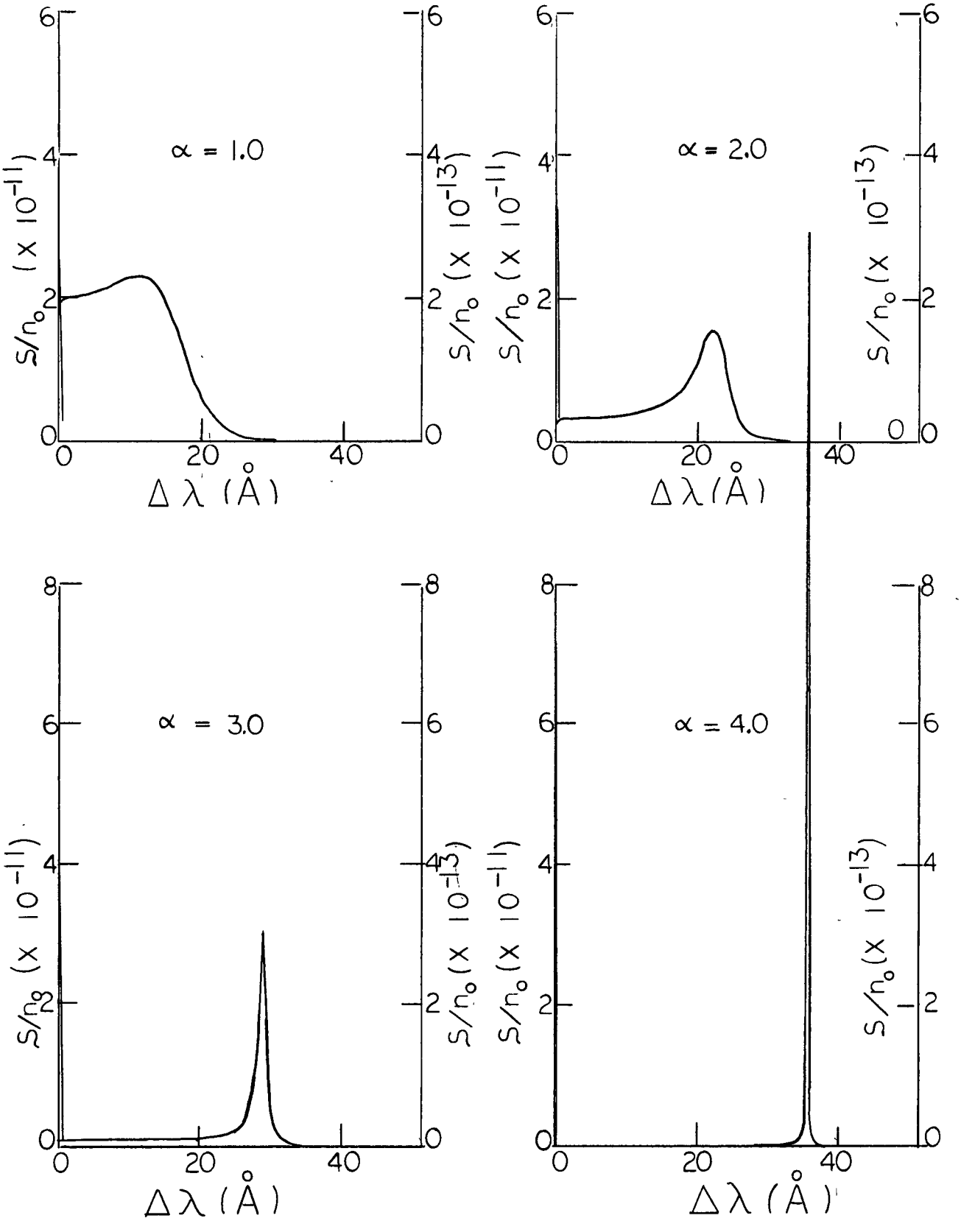


Fig. 4: Theoretical Scattered Spectrum for $\alpha > 1$ calculated for Argon Plasma with Z = 1, $T_e$ = 13,500°K, $\Theta$ = 45°

a Lorenztian shape like equation (27). This sharp resonance represents the so-called positive-ion oscillations, whose frequency is the same as that of a plasma oscillation for a ficticious particle with ion charge and mass but with electron temperature. The positions of these resonances are given by a similar dispersion relation to (26),

$$\omega_0'^2 = \frac{\omega_{pi}^2}{1+\alpha^2} + \frac{3kT_i k^2}{m_i} \tag{33}$$

where $\omega_{pi}$ is the plasma frequency defined for the ions.

To summarize: For small $\alpha$ ($\lambda \ll \lambda_D$), the scattered spectrum shows a Gaussian profile whose width is characterized by the electron thermal velocity. The effective scattering cross-section equals the Thomson scattering cross-section. For large $\alpha$ ($\lambda \gg \lambda_D$) the scattered spectrum consists of a central peak whose width is characterized by the ion thermal velocity and two "satellites" separated from the central peak by approximately $\omega_p$, the frequency of electrostatic oscillations in the plasma. The width of the "satellites" is controlled by Landau Damping. The total intensity scattered is equal to $\frac{1+\alpha^2}{1+2\alpha^2}$ of the Thomson value. The ratio of the integrated intensity of each satellite to the central peak is $\alpha^{-2}$.

## CHAPTER III GENERAL EXPERIMENTAL CONSIDERATIONS

A typical experimental arrangement for observing scattered light consists of a laser as the light source, a plasma as the scatterer, and an analyser system such as a monochromator and photomultiplier combination. Despite the fact that a very powerful laser beam is used for the incident radiation, the scattered signal is difficult to observe both because of the small scattering cross-section and because of the presence of large amount of noise due to extraneous light. There are two sources of this undesired light: The stray light due to reflection of the incident light from walls and windows of the apparatus and foreign particles and the emission from the plasma itself. In addition the detector noise also sets a low limit to the intensity of light that can be measured. Section A is devoted to estimating the size of the scattered signal, while in Section B the main sources of noise are discussed. In Section C proposals for optimizing the signal to noise ratio ($S/N$) are discussed.

### (A) Signal of Scattered Light

A quantitative measure of scattering is conveniently expressed by the ratio of the power scattered by the plasma in a given direction to the energy flux density of the incident radiation. This ratio has the dimension of area and is called the effective scattering cross-section defined by

$$d\sigma \equiv \frac{d\bar{P}}{\bar{I}} \qquad (1)$$

where the bar means a time average.

$d\bar{P}$ is the energy scattered by the plasma into the solid angle $d\Omega$ per sec. and $\bar{I}$ the Poynting flux of the incident wave.

For a monochromatic polarized beam incident on a free charge at rest, the quantity $d\sigma$ has been calculated[19] to be

$$d\sigma = \frac{e^2}{mc^2} \sin^2\gamma \, d\Omega \qquad (2)$$

where $\gamma$ is the angle between the scattering direction and the incident $\underline{E}$ field.

If U is the total energy of the laser pulse with a time duration, t focused into an area A, then

$$\bar{I} = \frac{U}{At} \qquad \text{ergs sec}^{-1}\text{cm}^{-2} \qquad (3)$$

$$= \frac{U}{h\nu At} \qquad \text{photons sec}^{-1}\text{cm}^{-2}$$

where $h\nu$ is the energy of an incident photon.

If the scattering volume $d\tau = A.l$ where l is the length of the scattering plasma volume and $n_e$ is the electron density, then

$$d\bar{P} = \frac{U}{h\nu . t} r_0^2 \sin^2\gamma \cdot l \cdot n_e \, d\Omega \qquad \text{photon sec}^{-1} \qquad (4)$$

$$= \frac{U}{h\nu} r_0^2 \sin^2\gamma . l \; n_e \, d\Omega \qquad \text{photons per pulse}$$

Equation (4) gives the number of photons scattered into the solid angle $d\Omega$ from one laser pulse. For a system of electrons which are moving as in a plasma, the scattered profile will be broadened depending on the parameter $\alpha$ according to the manner described in Chapter II. A detector, such as a monochromator and photomultiplier will see only a fraction of the photons given in equation (4) depending on the bandpass of the detector and the particular part of the scattered spectrum under observation. If this fraction is h and if q is the quantum efficiency (in electrons per photon) of the photomultiplier, then the current at the photocathode of the photomultiplier is

$$i_p = \frac{U}{h\nu t} r_0^2 \sin^2\gamma \cdot l \cdot n_e \cdot e \cdot h \cdot q \cdot d\Omega \qquad \text{amps} \qquad (5)$$

Numerical Example

Power of Laser = 10 MW (1/2 joule in 50 ns)

Area of focused beam = 0.5 mm x 0.5 mm

Length of plasma colume = 2 mm

Electron density = $10^{16} cm^{-3}$

Solid angle = .01 steradian (i.e. f/10 monochromator)

Quantum efficiency for a S20 photocathode surface at 7000 A = 3% (.03 electron per photon) According to (5), the photocathode current $i_p = h10^{-7}$ amps. Even at the satellites, for an $\alpha$ of 5, ($h \simeq 1/50$), the photocathode current $i_p = 2 \times 10^{-9}$ amps. If the gain of the photomultiplier $G = 10^5$, the output current at the anode is a few tenths of a milliamp. and should be easily measurable. The difficulty does not lie so much in the smallness of the signal as in the large noise background against which one observes the signal.

(B) Extraneous Signals and Noise

The main sources of extraneous signals are the stray light from the laser, that is the laser light which enters the detector without being scattered by the plasma, the self-radiation of the plasma and the noise from the detector itself.

(i) Stray Light from Laser

The source of light is a very powerful beam so that reflections from walls and windows and foreign particles will be serious. Unless special precautions are taken, extraneous signals due to the stray light will mask the scattered signal which is typically a factor $10^{-12}$ of the incident light.

(ii) Plasma Luminosity

The emissions from the plasma include largely (a) bremstrahlung radiations which are transitions between free state of electrons moving in the Coulomb fields of the ions (free-free transitions), (b) recombination radiations due to free-bound transitions and (c) line radiations (bound-bound transitions). In general these all depend in complicated ways on the temperature, electron density, degree of ionization and the dynamics of the plasma.[20]

(iii) Statistical Fluctuations

These are from two sources: (a) the shot noise caused by the discrete number of photons which release electrons from the cathode of the photomultipliers and (b) the shot noise in the photocathode current itself since the current is a flow of discrete electrons. When a photomultiplier is not exposed to light, it shows a dark current which is thermal in nature, and the shot noise of this current is given by[21]

$$\langle i^2 \rangle = 2 e i_d \Delta f \qquad (6)$$

where e is the electron charge, $\Delta f$ the bandpass of the amplifier and $i_d$ the dark current. In the presence of light this expression becomes

$$\langle i^2 \rangle = 2 e (i_d + i_T) \Delta f \qquad (7)$$

where $i_T = i_p + i_{stray} + i_L$ is the total light current at the photocathode,

$i_p$ is the current due to scattered light,

$i_{stray}$ is the current due to stray light of laser

and $i_L$ is the current due to the plasma luminosity.

(C) Signal-to-noise

(i) Improvement of Scattered Signal

An absolute increase of scattered signal naturally improve the S/N ratio. This can be achieved by using a high power laser to increase the number of incident photons, by a dense plasma to increase the number of scattering electrons and a high speed monochromator to increase the solid angle over which the scattered light is gathered, (an interference filter could be used in place of a monochromator, allows collection of more light). However since scattering is a function of angle, the f-number cannot be increased indefinitely.

(ii) Reduction of Stray Light

Suitable baffles and light traps should be provided to reduce the stray light. It is desirable to first focus the laser to a small spot and allow the image to pass through a pin hole to eliminate extraneous light from the laser. The baffling is largely an experimental problem and each case has to be treated individually. The eye is most useful in detecting the source of stray light. If windows are present as is usually the case, they should be placed at the Brewster angle so that the linearly polarised laser light is not reflected. A monochromator with small stray ratio is very useful for reduction of stray light provided the part of the spectrum observed is far from the central wavelength of the laser line. A double monochromator such as the one used by Davies and Ramsden[15] would in principle reduce the stray light ratio by the square of this ratio. In addition a red filter may be used to prevent second order stray light from

entering the detector.

(iii) Reduction of Shot Noise

We observe from (7) that the root mean square of the shot current at the anode of the photomultiplier is

$$\langle I^2 \rangle^{\frac{1}{2}} = G [ 2 e \Delta f (i_d + i_T) ]^{\frac{1}{2}} \tag{8}$$

where G is the gain of the photomultiplier.

The total photon-current at the anode is

$$I_T = G \, i_T \tag{9}$$

so that the figure of merit F is given by

$$F = \frac{I_p}{\langle I^2 \rangle^{\frac{1}{2}}} = \frac{i_p}{[2 e \Delta f (i_d + i_T)]^{\frac{1}{2}}} \tag{10}$$

This ratio will improve if $i_p$ is large so that a photomultiplier with a high quantum efficiency at the laser wavelength should be used. There is a limit in the reduction of the bandwidth $\Delta f$ of the amplifier because the laser pulse is a very fast pulse. If the dark current $i_d$ is significant, a photomultiplier with low dark current should be used, and the tube cooled with liquid nitrogen or dry ice.

(iv) Reduction of Plasma Luminosity

The kind of gas used in the plasma is quite an important consideration in designing a scattering experiment. In general hydrogen or helium should be used, firstly because they have relatively few lines in the neighbourhood of the laser line. Secondly, the continuum background which is mainly bremsstrahlung and recombination radiation, increases as the square of the ionic charge, the heavier elements will produce intense continuum at high temperatures at which multiple ionization occurs.

Cleanliness of the plasma is also important as any solid particle or dust will have a much larger scattering scross-section than electrons. These will increase the stray light at the laser frequency. Scattering from neutral atoms and molecules may sometimes be significant. The scattering cross-section for neutral atoms and molecules is given by the Rayleigh Scattering law[22] and is related to the refractive index by

$$\sigma = \frac{32}{3} \pi^3 \lambda^{-4} n_o^{-2} (\mu - 1)^2 \qquad (11)$$

where $\sigma$ is the Rayleigh scattering cross-section

$n_o$ is the density of neutral atoms or molecules and

$\mu$ the refractive index

Roughly the cross-section is about .003 of that of the electrons and when the ionization is not high, this will cause significant changes in the intensity at the laser frequency.

(v) Reduction of Electrical and Magnetic Pick-up

Electrical and magnetic pick-up can be a serious problem especially in plasma physics work where high current discharges are common. Hence all measuring apparatus should be properly shielded to prevent electrical pick-ups from spark gaps, etc. and any complete loop in electrical connections should be avoided to prevent magnetic pick-up.

(vi) Sampling Technique

If the signal-to-noise ratio is still low, a sampling technique may be used. Essentially this technique averages a sample of results. The noise, being a random source will tend to average out whereas the signal will not. By taking a sufficiently large sample, the signal-to-noise ratio may be considerably improved; it increases as the square root of the number of the samples.

## CHAPTER IV SCATTERING FROM Θ-PINCH

Much work has been done on the Θ-pinch recently because of the possibilities of creating a high temperature plasma of thermonuclear interest. A knowledge of the densities and temperatures of the electrons and ions would be very useful toward a better understanding of the behaviour of the plasma. The Θ-pinch plasma is also very suitable for demonstrating light scattering because it is reasonably clean and has high electron density and temperature. A high electron density will naturally increase the scattered signal, whereas a high temperature plasma is advantageous because the scattered profile will be Doppler broadened so that observations can be made at frequencies where the intensities of the stray light may be expected to be small.

### (A) Apparatus and Procedure

#### (i) The Θ-Pinch

A schematic drawing of the Θ-pinch discharge is shown in Fig. 5. The condenser bank consists of five 5-μf 20KV NRG low inductance capacitors normally charged to 12KV through a high voltage power supply (20KV,50ma). The voltage across the bank is measured to ± 250v with a microammeter connected in series with a 500M resistance.

The discharge vessel (see Fig. 6) consists of a 2 in. diameter pyrex glass tube two feet long. The Θ-pinch coil is made of copper 1/32 in. thick and 5 in. wide wrapped tightly round the glass tube. A slit of 1 cm x 1 mm is cut in the copper coil to allow transverse observation to be made. The vessel is provided with two Brewster windows at both ends of the tube and green

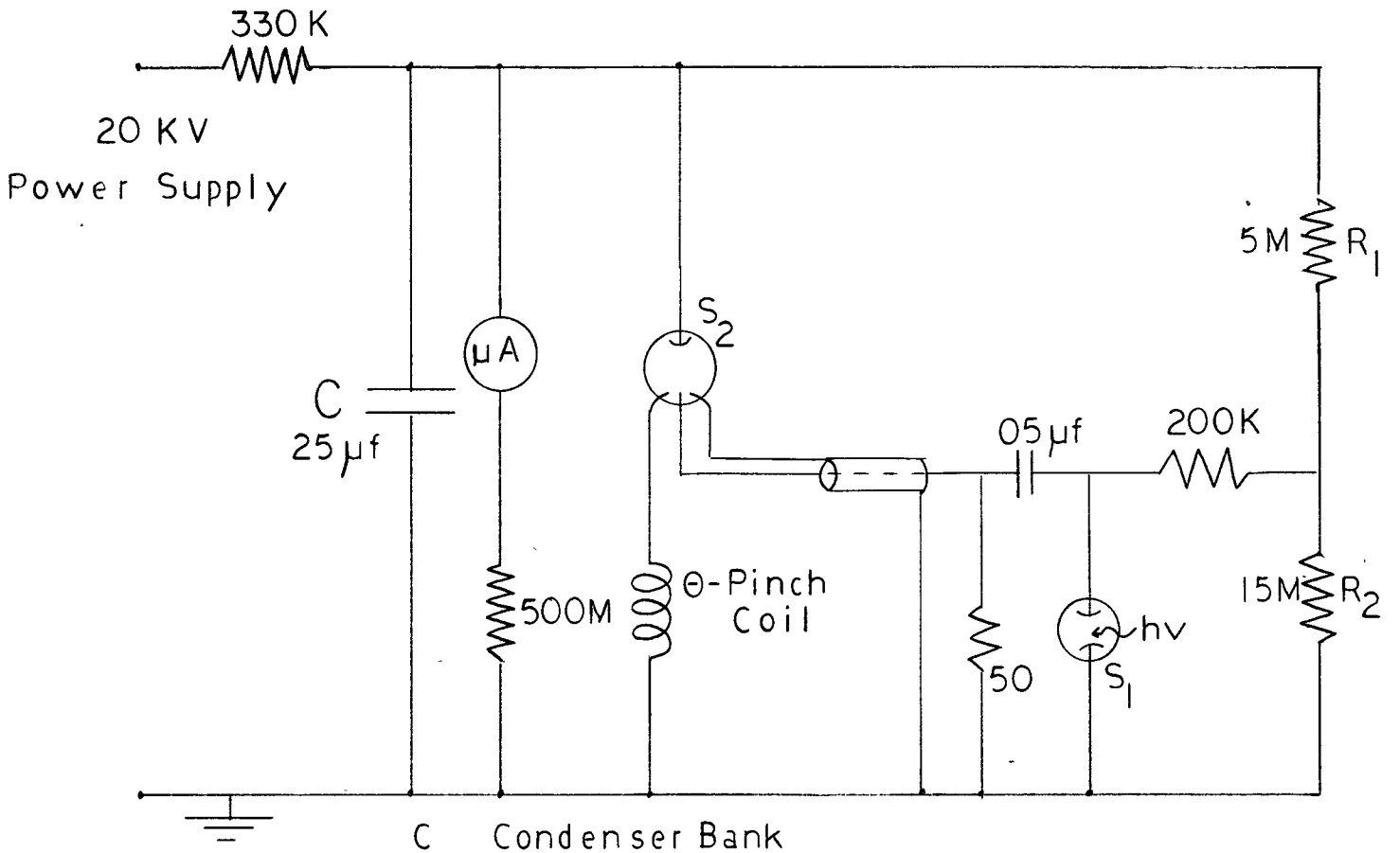


C Condenser Bank
$R_1$ $R_2$ Potential Divider
$S_1$ Ultra violet Trigger Spark Gap
$S_2$ O Pinch Bank Spark Gap
μA Microammeter

**Fig. 5: Schematic Drawing of Θ-Pinch Discharge**

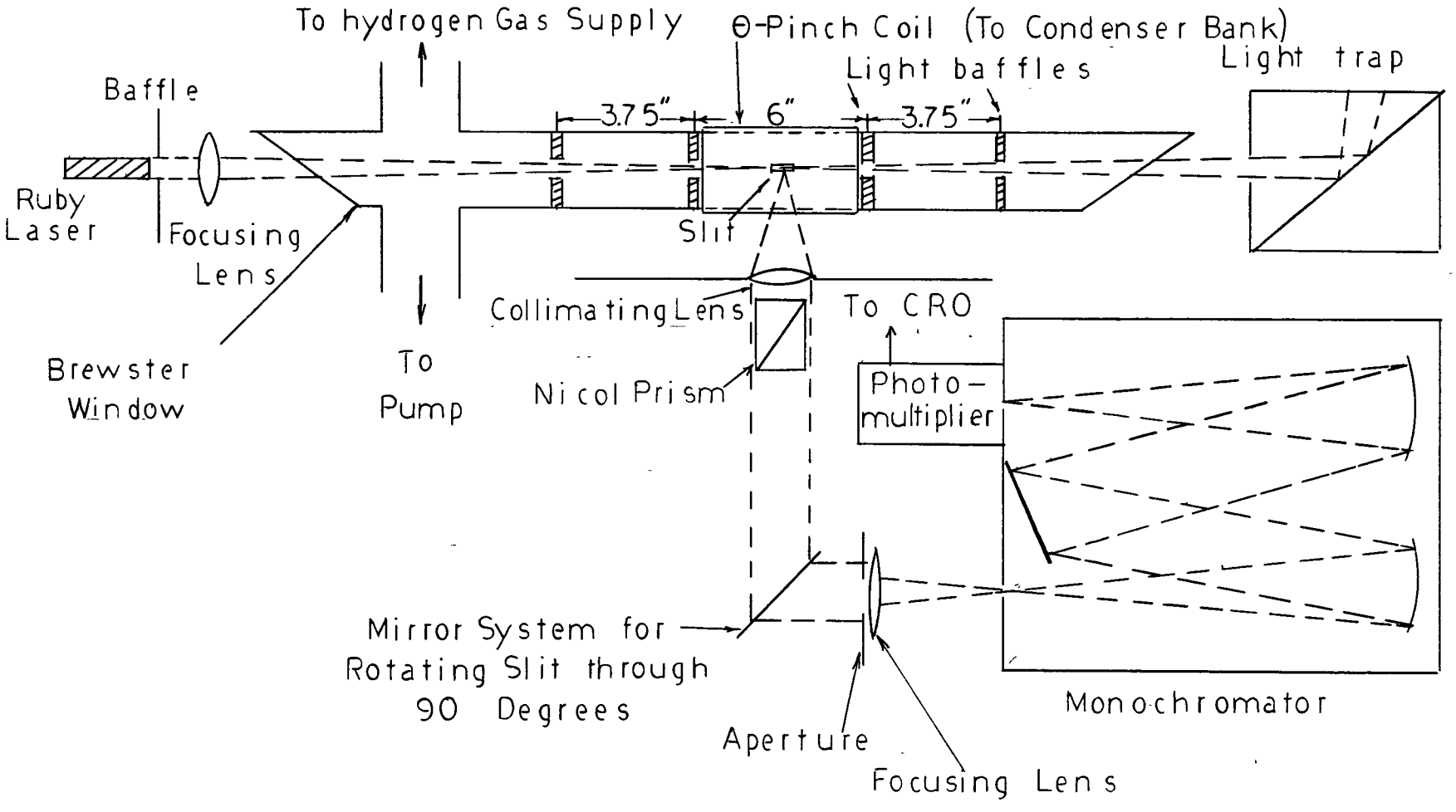


**Fig. 6: Schematic Drawing of Scattering Apparatus (Θ-Pinch)**

glass discs (with holes of diameter 1/2 in. in the centre) are placed inside the tubing to reduce the stray light reflected from the glass wall. The vessel is evacuated by a fore-pump and a diffusion pump so that the system can be pumped down quickly after each discharge. The pressure is measured with a Pirani gauge calibrated by a Mcloed gauge.

Fig. 7 shows a block diagram of the trigger system. A fast-rise synchronisation pulse ( +4v, 10 μs duration ) which occurs at 77 μs before the laser operates is first passed through a phase inverter which changes it into a negative pulse for triggering the following variable delay unit. The delay time of the delay unit is variable from 1 μs to about 1 ms. The output from the delay unit, which is a pulse of + 40v and 10 μs duration, is used to fire a thyratron unit. The thyratron trigger unit sends out a 9.5 KV pulse into a Theophanis termination[23] which presents a large impedance to the pulse and doubles its amplitude to 19 KV with a rise time of 40 ns. This pulse is used to trigger an ultra-violet (UV) trigger generator[24].($S_1$ of Fig. 5). The UV trigger generator has the advantage that it isolates the Theophanis unit from the main condenser bank and thus reduces electrical pick-up. When the UV gap breaks down it sends out another trigger pulse which breaks down the main spark gap ($S_2$ of Fig. 5), causing a surge current and ionising the gas in the pinch-tube. The overall triggering is accurate to few tenths of a microsecond. Most of the jittering is from the variable delay unit.

The discharge current is measured with a Rogowski coil made from a loop of RG 65 A/U delay line. It is a form of current transformer where the secondary is the toroidally wound coil

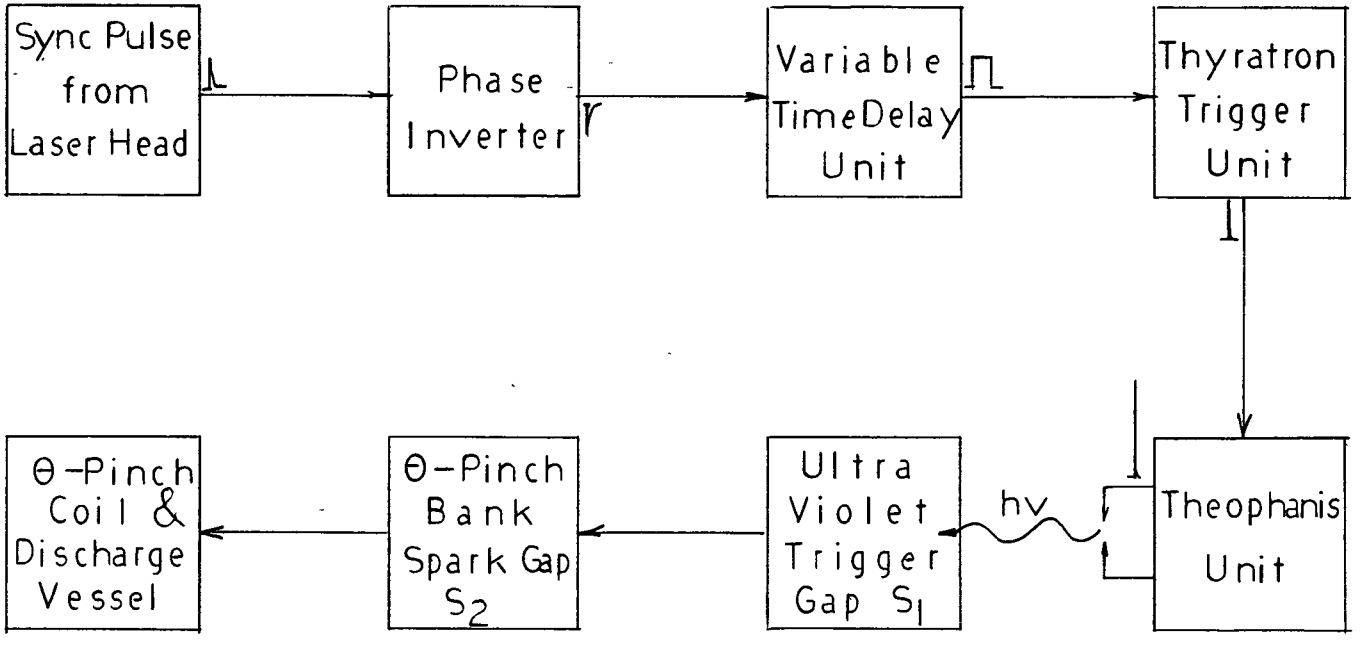


**Fig. 7: Block Diagram of Trigger System**

through which the magnetic field of the main discharge current (the primary) is threaded. The maximum value of dI/dt is $10^{11}$ amp/sec. reached in times of $10^{-6}$ sec., giving a peak current of order $10^5$ amps. The current waveform of the discharge is shown in Fig. 8a. It is obtained by integrating the signal from the Rogowski coil through an integrator of RC time constant of 100 μs. The light output of the plasma is also shown in Fig. 8b.

(ii) The Laser

A TRG-104 giant pulse laser with peak power of 10 MW centred at 6943Å, and 50ns duration is used. The giant pulse is achieved by rotating a prism at a speed of 30,000 rpm. The beam has a divergence of 10 milliradian and the output is linearly polarized in the vertical direction. The laser output is monitored by a RCA 922 fast-rise photodiode and the output power is reproducible to ± 10% provided that the laser is fired at regular intervals of about 4 pulses a minute or less.

(iii) The Monochromator

A Jarrell-Ash Ebert monochromator (82-010) with a Bausch and Lomb grating (35-00-58-38) is used. The grating has a ruled area of 2 in x 2 in and has 30,000 grooves/in., blazed at 7500 Å. The linear dispersion of the instrument corresponds to 16A/mm and the speed is f/10. The wavelength is calibrated with a Hg light source and is accurate to half Å. The monochromator, as manufactured, has a stray light background of 1.6%. We have lined the inside with black flock-paper and added additional baffling to improve this ratio to about .3%. This figure is obtained by measuring the stray light of the laser at 6943Å and at wavelengths outside the bandpass of the monochromator slit which is set at 8Å.

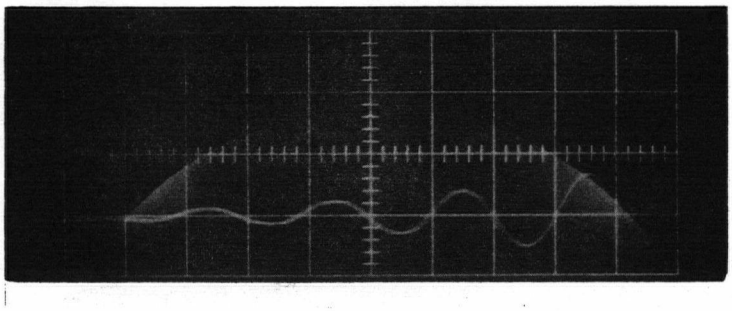

(a)

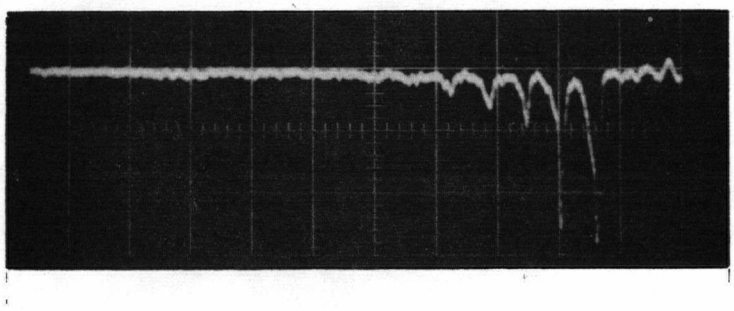

(b)

← time

Fig. 8: (a) Current Waveform
Time Scale: 5 μs/cm
Voltage Scale: 5 v/cm

(b) Plasma Light Output
Time Scale: 10 μs/cm
Voltage Scale: .1 v/cm

For a 10 μ slit, the instrument has resolution at least equal to .2 Å in the first order.

(iv) The Photomultiplier

The photo-detector is a Philips CVP 150 photomultiplier with an S1 photocathode surface with a quantum efficiency of about .4%. (At the time that the experiment was performed a S20 photocathode surface was not available). The photomultiplier circuitry is shown in Fig. 9a. The linearity of the tube has been tested both under pulsed (laser) light and d.c. light conditions. Fig. 9b shows the calibration curves. It is found that the response is linear up to 30ma in the pulsed condition and about 2 ma with d.c. light. The photomultiplier is normally operated at 14KV and the r.m.s. ripple voltage of the photomultiplier power supply is 5mv.

(v) The Optics

With reference to Fig. 6 again where is shown the schematic diagram of the optical arrangement. The laser light is passed through a light baffle aperture of diameter 1 cm before it is focused by a lens of focal length 20 in at the centre of the discharge tube. (Geometry of the tube does not permit use of a shorter focal length lens) The diameter of the focused spot is about 1 mm. A light trap in the form of a big black box is placed at one end of the discharge tube opposite to the laser to catch the transmitted light and prevent it being reflected into the detector.

Scattered radiation is picked up at $90^{o}$ by a collimating lens (f = 5.4 in). The image of the slit in the copper coil, which is horizontal, is rotated through $90^{o}$ by a front-surface

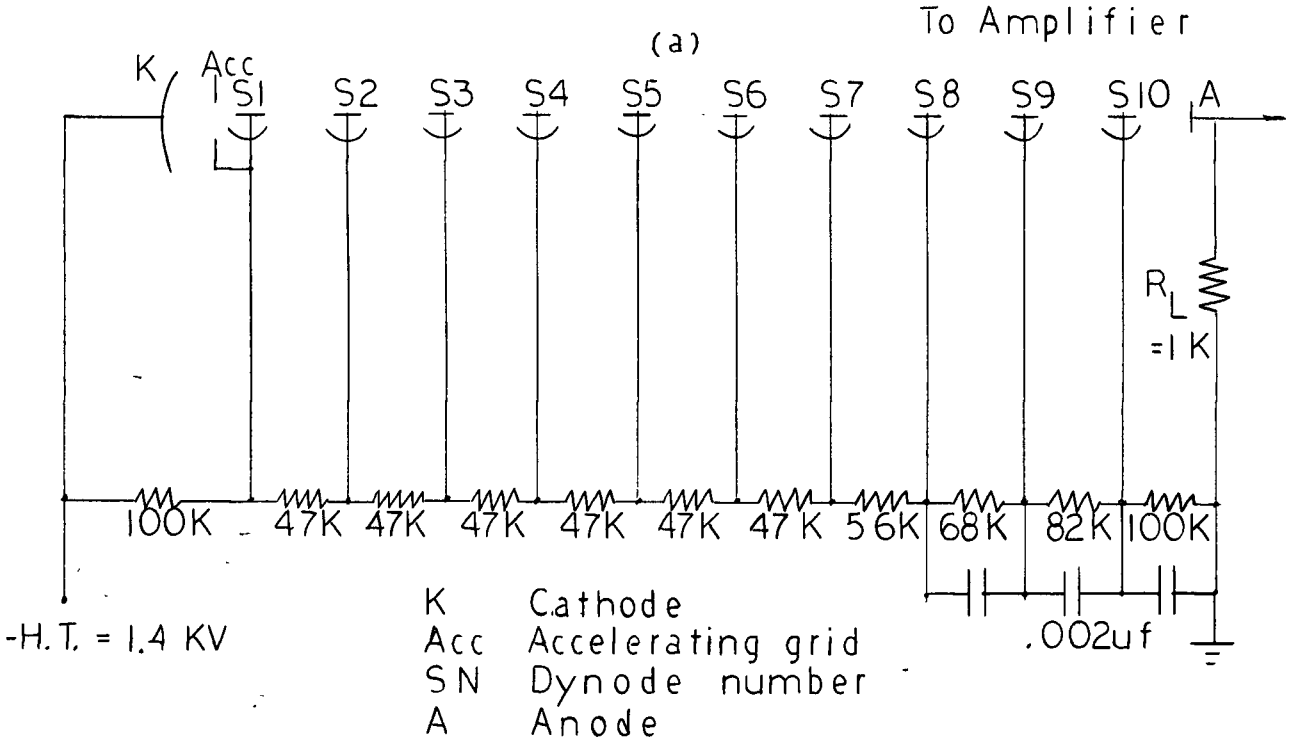


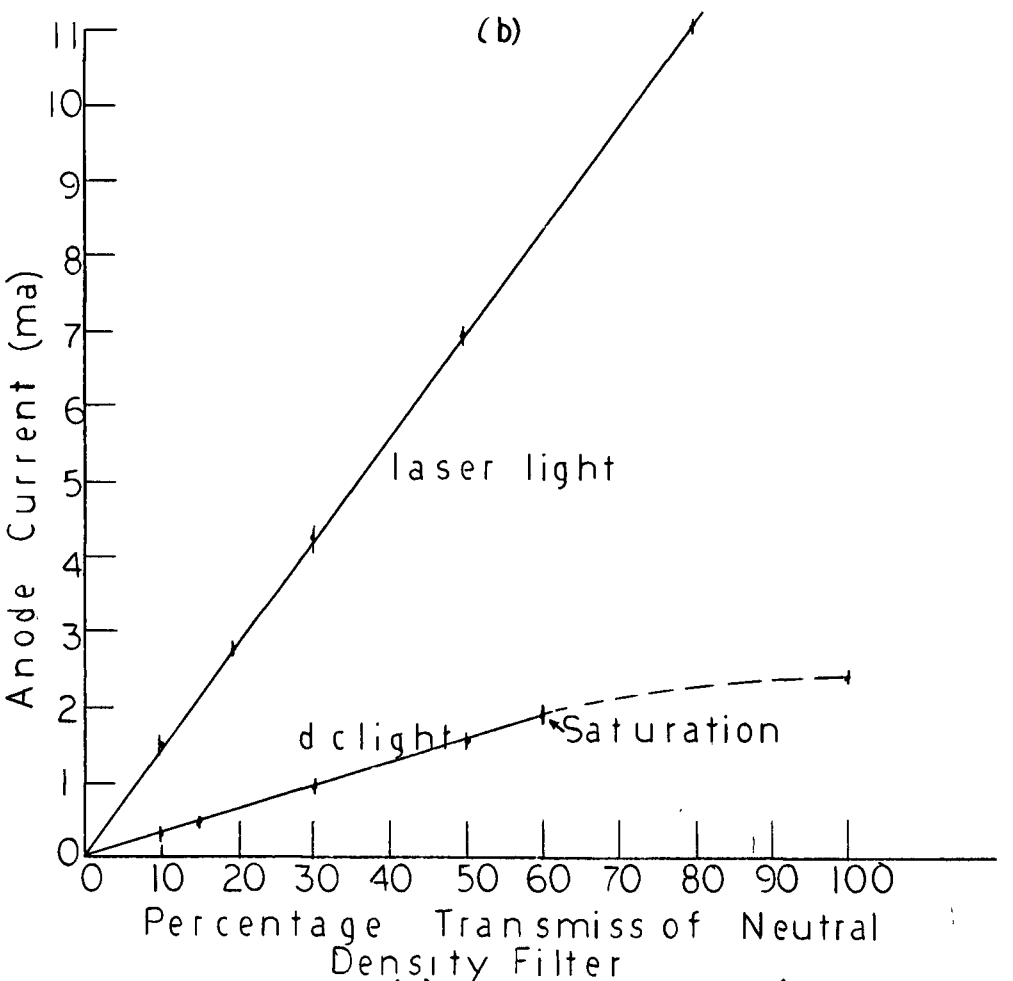


**Fig. 9: (a) Photomultiplier (Philips CVP 150) Circuitry**
**(b) Linear Response of Photomultiplier**

mirror system to the vertical direction so that it can be imaged by another lens (f = 5.4 in) on the entrance slit of the monochromator. The slit height is 10 mm and the slit width is set at .5 mm corresponding to 8Å passband. The maximum amount of useful light that can be sent into a monochromator is limited by the f-number of the instrument. For a given light source, the maximum amount of useful light that can be sent into the instrument is obtained when the grating is 'flooded' with light. In our present application, because the light source (the scattering plasma volume) is finite and small and remote from the entrance slit of the monochromator, a system of lenses is required to image the source onto the slit so as to fill the monochromator grating with light. The optical magnification is unity because there is no point in obtaining greater illumination at the monochromator slit unless it is accompanied by greater flux per unit solid angle or by a greater useful angle. The volume of the plasma observed will be determined by the size of the image of the slit together with the size of the focused laser spot.

To align the system, a pin having approximately the size of the scattering plasma volume is placed inside the pinch-tube to represent the plasma which scatters the light. A light source is placed at the exit slit of the monochromator and its image is lined up with the pin by the method of no parallax. The laser, which can be adjusted both vertically and horizontally, is then made to focus on the pin.

Light baffles are provided throughout and in particular an aperture is placed in front of the monochromator so that no extra light is sent into the instrument, increasing the stray light.

With these precautions, the ratio of the incident light to the stray light is of the order of $10^{11}$. This ratio is obtained by measuring the intensity of the incident laser light (reduced by neutral density filters) which is approximately $2 \times 10^{12}$v and the intensity of the stray light by the same photomultiplier which is approximately 2 x 10v. Even so the stray light at the centre frequency (20v) is about 100 times the expected scattered signal which is about .1v, and measurements have to be taken such that the central wavelength of the laser is outside the bandpass of the monochromator slit. In addition the stray light background profile of the monochromator shows some wavelength dependence probably due to grating ghosts. This stray light is subtracted from the total signal to give the scattered signal.

(B) Experimental Results

The experimental conditions are tabulated as follows:

| | |
|---|---|
| Gas used | Hydrogen |
| Pressure of gas | 150 μ of Hg |
| Stored energy of condenser bank | 1.5 KJ |
| Time of observation | 44 μs after initiation of discharge, i.e. in the after-glow |
| Observation angle | $90^{\circ}$ |
| Solid angle over which light is collected | .01 steradian |
| Observed plasma volume | 10 mm x 1 mm x .5 mm |
| Bandpass of monochromator slit | 8Å (500 μ slit) |

Fig. 10 shows some typical oscilloscope traces and in Fig. 11 the experimental results are plotted for the scattered intensity versus the wavelength setting of the monochromator. Each point on the graph (Fig. 11) is an average of four experimental

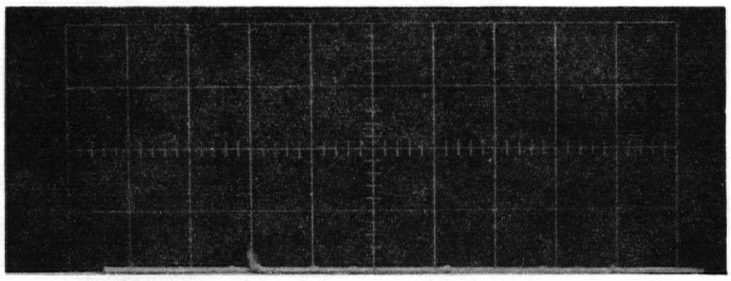

(a)

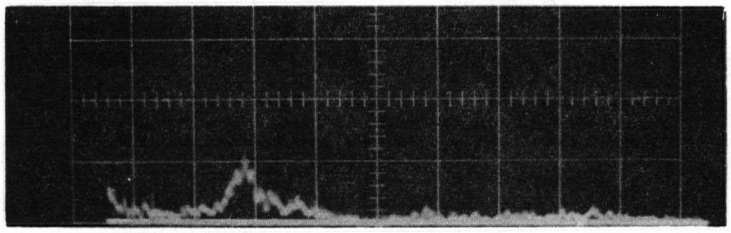

(b)

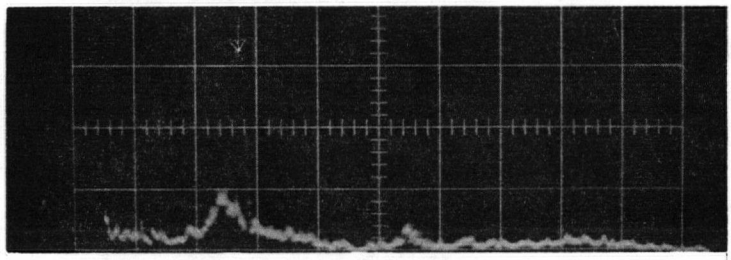

(c)

Fig. 10: Typical Oscilloscope Traces (Θ-pinch)
(a) Laser alone
(b) Plasma alone
(c) Laser and Plasma
Time Scale: 2 μs/cm delayed by 70 μs
Voltage Scale: 0.1 v/cm
$\lambda$ = 6930Å

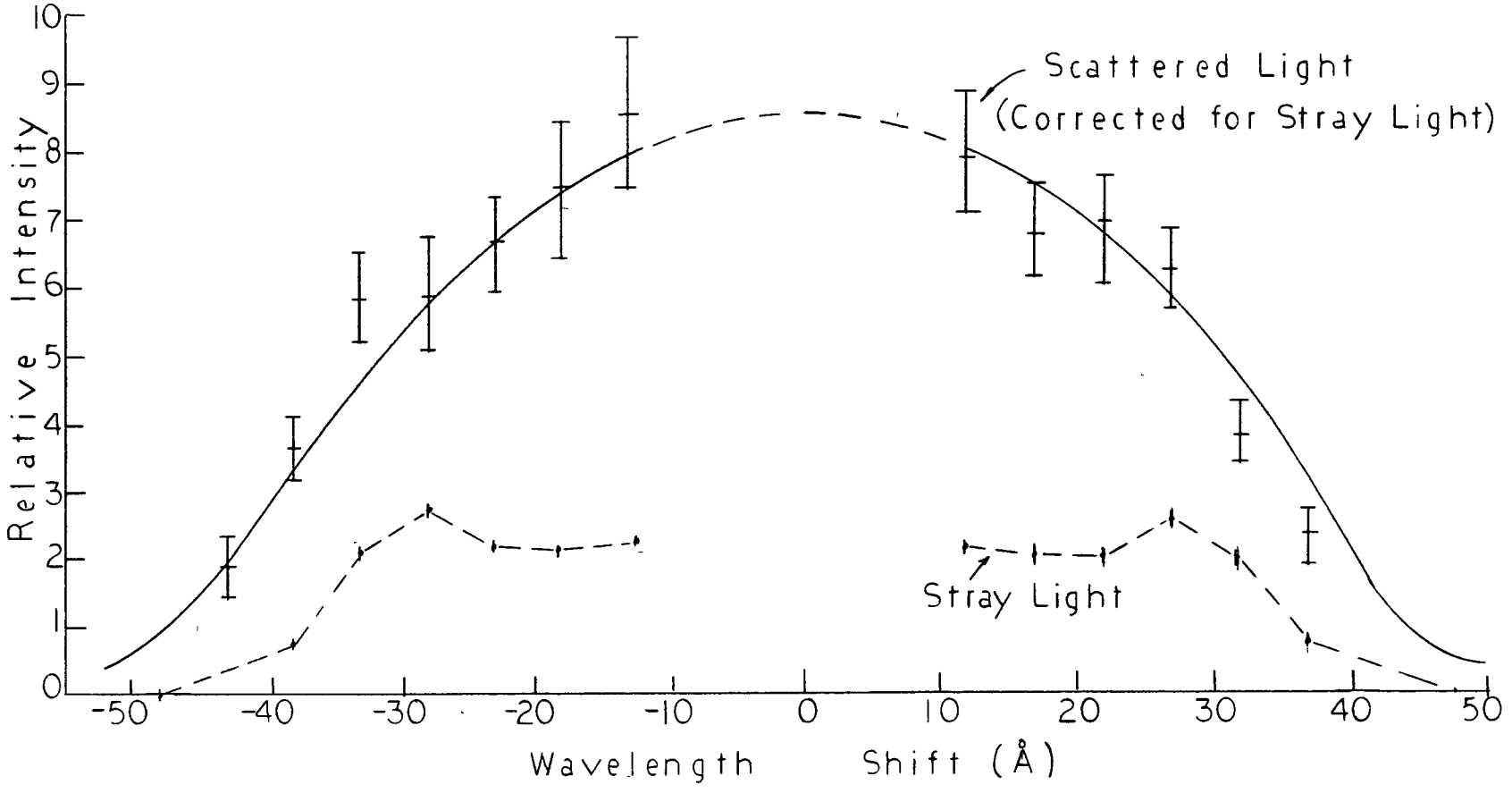


Fig. 11: Scattered Spectrum of Laser light by Θ-pinch Plasma
Vertical Scale: 4 divisions = .1v

determinations and the vertical bars represent the standard deviations of the mean. The scattered profile shows a nearly-Gaussian shape with a fairly flat top. A least squares fit of the theoretical curve (equation 20 of Chapter II) to the experimental points shows that $\alpha = .61 \pm .20$, $T_e = 25{,}000^{\circ}$ K $\pm$ $6{,}000^{\circ}$ K and $n_e = (1.0 \pm 0.3) \times 10^{16} cm^{-3}$. Also shown on Fig. 11 is the theoretical best fit (solid curve).

It is seen that there is significant scatter of the experimental points. This is thought to be due largely to the local non-reproducibility of the plasma. For $\alpha < 1$, the scattered spectrum is not very sensitive to $\alpha$ and therefore the determination of the above parameters cannot be very accurate. In order to determine this parameter more accurately, it would be desirable to arrange experimental conditions such that $\alpha > 1$ and determine them from the positions of the satellites.

A forward scattering experiment has been attempted to observe these satellite lines, but the large amount of stray light masked the signal. Although it is possible to reduce the stray light, it was decided that a plasma jet would be much more suitable for the purpose of seeing the satellites. The work with the plasma jet is described in the subsequent chapter.

## CHAPTER V SCATTERING FROM PLASMA JET

In order to observe the satellite lines with a Θ-pinch plasma, one has to make observation of the scattered light at a very small angle ( a few degrees ). Because of the enormous amount of stray light encounted, it was thought that another plasma might be more suitable. A plasma jet was chosen because it is fairly simple to obtain a reproducible plasma with an electron density of $10^{16}$ to $10^{17}$ $cm^{-3}$ at an electron temperature of 1 or 2 ev if argon is used as the working gas [25]. These conditions make it possible to observe satellites at a large scattering angle. It is much easier to reduce the stray light when making observations at this large angle as compared with small angle forward-scattering. In addition, since the jet is operated at atmospheric pressure, we need no windows or walls in the neighbourhood of the plasma which again reduces stray light problem. The apparatus can also be arranged to vary the observation angle.

### (A) Apparatus and Procedure

#### (i) The Plasma Jet

The basic design of the jet and its associated power supply is shown in Fig. 12. It consists essentially of a tungsten cathode and a copper anode which is electrically grounded, both cooled by water. The system is mounted vertically in a brass can on an optical bench so that its position can be adjusted easily. A commercial welder unit ( Miller Model SRA-333 ),which delivers a current up to 300 amps. at 40 volts, was first used as the power source. It was found that it is unsatisfactory because the voltage ripple is about 16% of the output voltage

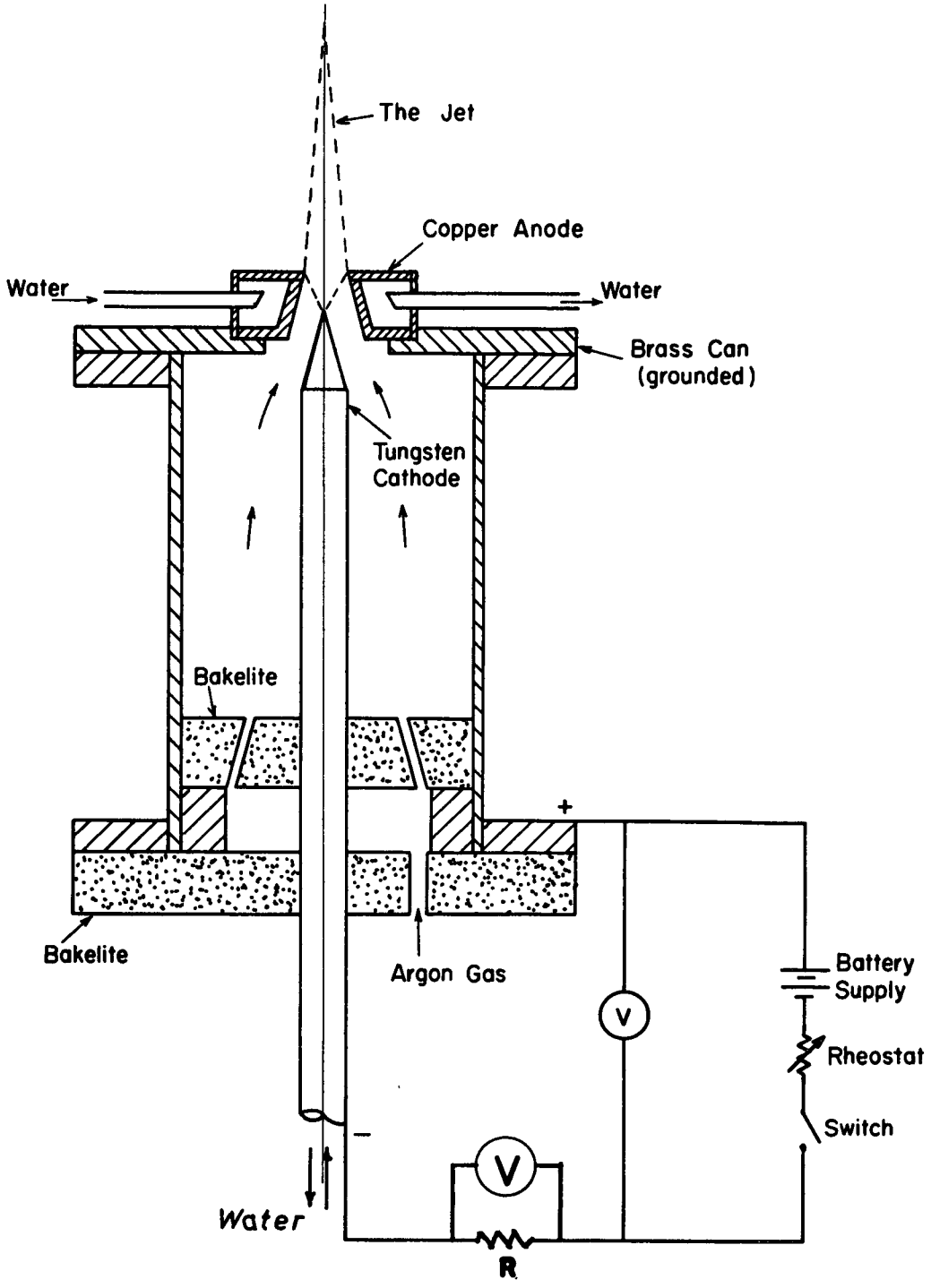


Fig. 12: The Plasma Jet

and the current ripple is about 33% when the jet is running at 200 amps. A total ripple of 50% in the light output was observed. Such a large fluctuation would alter the plasma parameters and so a battery supply was substituted.

The battery assembly consists of eight 12-volt heavy duty lead-acid batteries each rated at 200 amp-hours with internal resistance of a few milliohms. They are arranged in a 2x4 array ( 2 in parallel and 4 in series). A high power rheostat with variable resistance from 0.1 ohm to 0.4 ohm is placed in series with the batteries. The whole unit together is capable of delivering a current up to 300 amps. at 15 volts. The diameter of the anode is 5 mm and the tip of the cathode is set at 7 mm from the top anode surface. Argon is the gas used in the jet and the flow of the gas is controlled at a steady velocity of 15 m $sec^{-1}$ by a calibrated argon flow-meter. The voltage across the jet was measured with a voltmeter and the current by a heavy current shunt of resistance 0.25 milliohm in parallel with a voltmeter. The current-voltage characteristic of the jet is shown in Fig.13. The reading of the current was accurate to $\pm$ 4 amps. The jet extends to a distance of about 10 cm above the anode surface when the jet is running at 280 amps., but the intense spot is about 1 cm above the anode. The light output is a d.c. signal with a few percent fluctuation .

It should be mentioned that the welder power supply is used in running the jet except when an actual reading is taken. The welder is then switched off and the battery supply switched on for about 10 seconds to allow the current to reach a steady state before a reading is taken. The battery supply is then switched

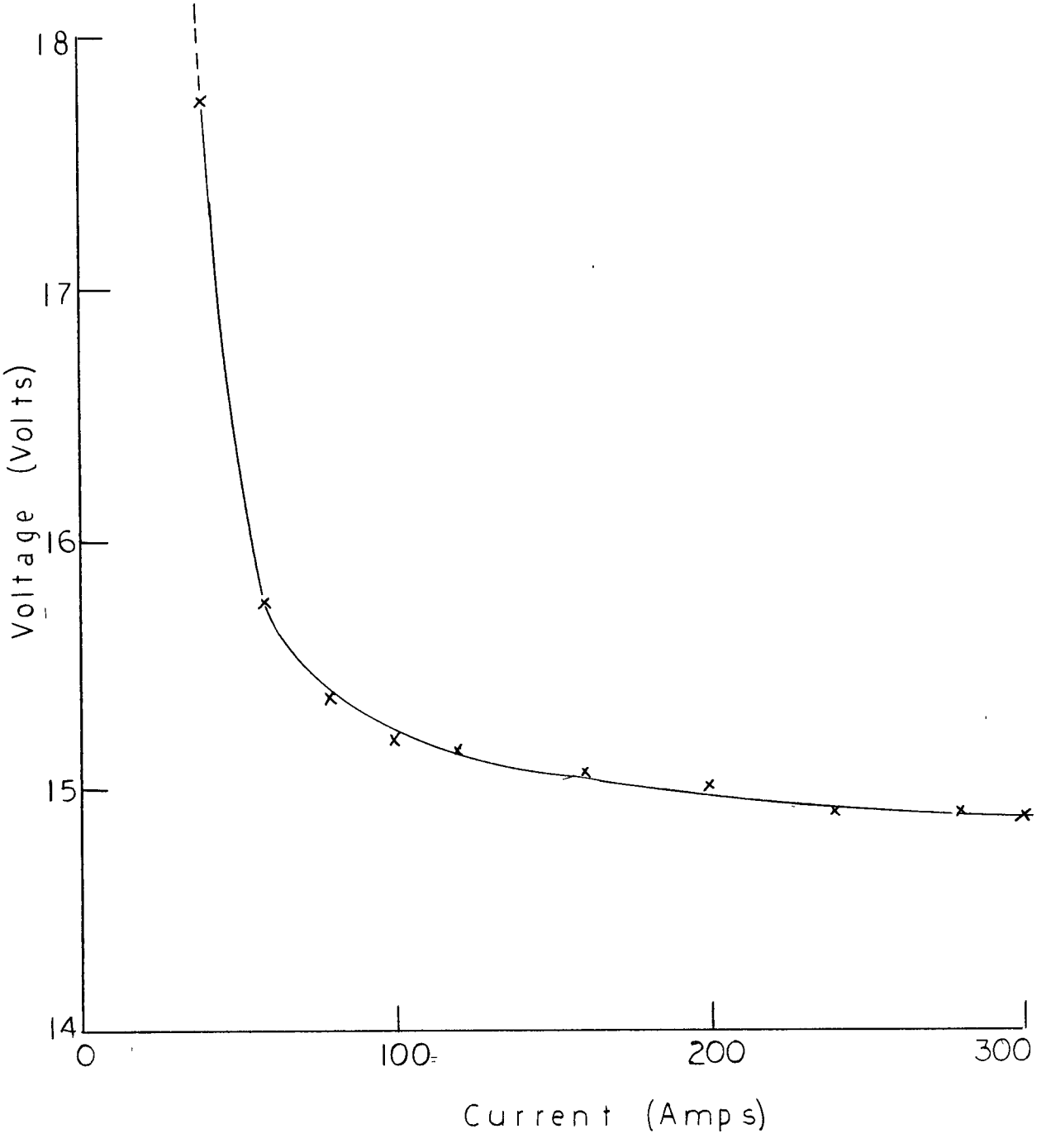


Fig. 13: Voltage-Current Characteristics of Argon Plasma Jet

off and the welder on until the next reading is taken, thus reducing the duty cycle of the batteries and keeping the jet in a fairly steady condition. The entire battery unit ( batteries and rheostat ) costs about $ 500 and has to be charged only occasionally, making it both very economic to build and not inconvenient to maintain.

(ii) The Optics

A schematic diagram of the optical arrangement is shown in Fig. 14. Much better baffling can be obtained in this case because there are no windows or walls in the vicinity of the plasma. The light from the laser is first focused by a lens of focal length 4 in. into a pin-hole (diameter 1/16 in.) and is then focused by another lens of focal length of 5 in. at the center of the jet at a height of 3 mm above the anode surface. Diaphragms are provided to prevent the incident beam hitting the anode surface. The incident light is trapped in a black box inside which is a fast-rise RCA 922 photodiode which monitors the light of the laser output and provides triggering for the oscilloscope. With these precautions the stray light background is now about 2 volts at the laser wavelength, representing a fraction of $10^{-12}$ of the incident beam. The stray light background of the monochromator has been studied carefully to avoid any instrumental effects, and it is negligible in the wavelength range we are scanning. The profile of the stray light is shown in a latter figure (Fig. 18) together with the scattered profile.

Scattered light is observed at $45^{o}$ from the forward direction. A field lens of focal length 2 in. collects the light and images it at a baffling slit of dimensions 2 mm x 0.5 mm.

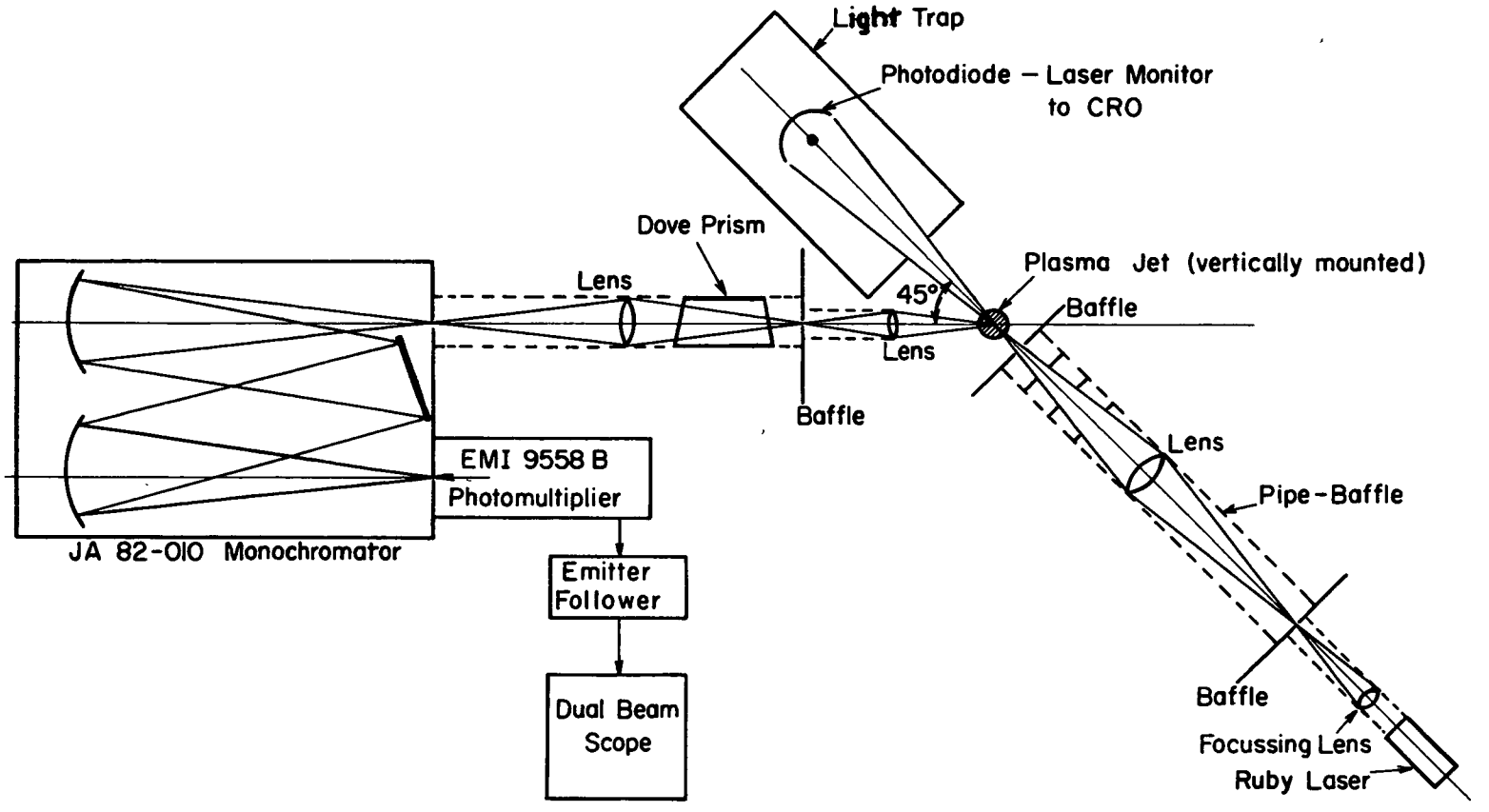


SCATTERING OF LASER LIGHT FROM A PLASMA JET

SCHEMATICS OF APPARATUS

Fig. 14: Scattering of Laser Light from a Plasma Jet(Schematics of Apparatus)

The light is then passed through a Dove prism which rotates the image through 90° and is focused at the entrance slit of the monochromator by another lens of focal length of 5 in. The slit height is 2 mm and the slit width is set at 0.5 mm corresponding to an 8Å passband. A greater length of the plasma is not selected because according to Ahlborn[26], the temperature of the plasma drops rapidly beyond a radial distance of 1 mm from the center of the jet. A HN 38 polariod and a Corning 52-63 red filter are also placed in front of the monochromator.

(iii) Photodetectors

Two photomultipliers were used, a Philips CVP 150 photomultiplier and an EMI 9558B tube. The latter has a quantum efficiency of about 3% at the laser wavelength as compared to 0.4% of the former, so that the signal-to-noise ratio for the shot noise of the phototube is expected to improve by a factor of 3. However the CVP 150 was used in earlier experiments before the EMI tube was available. The output from the photomultiplier is passed through an emitter-follower to maintain the time response of the circuit before being fed into a dual beam oscilloscope. Fig.15a shows the circuit diagram of the EMI photomultiplier and Fig. 15b shows its response curve. It is important to check that the photomultiplier is not saturated by the d.c. light background of the plasma.

(B) Experimental Results (Plasma Jet)

The experimental conditions are tabulated as follows:

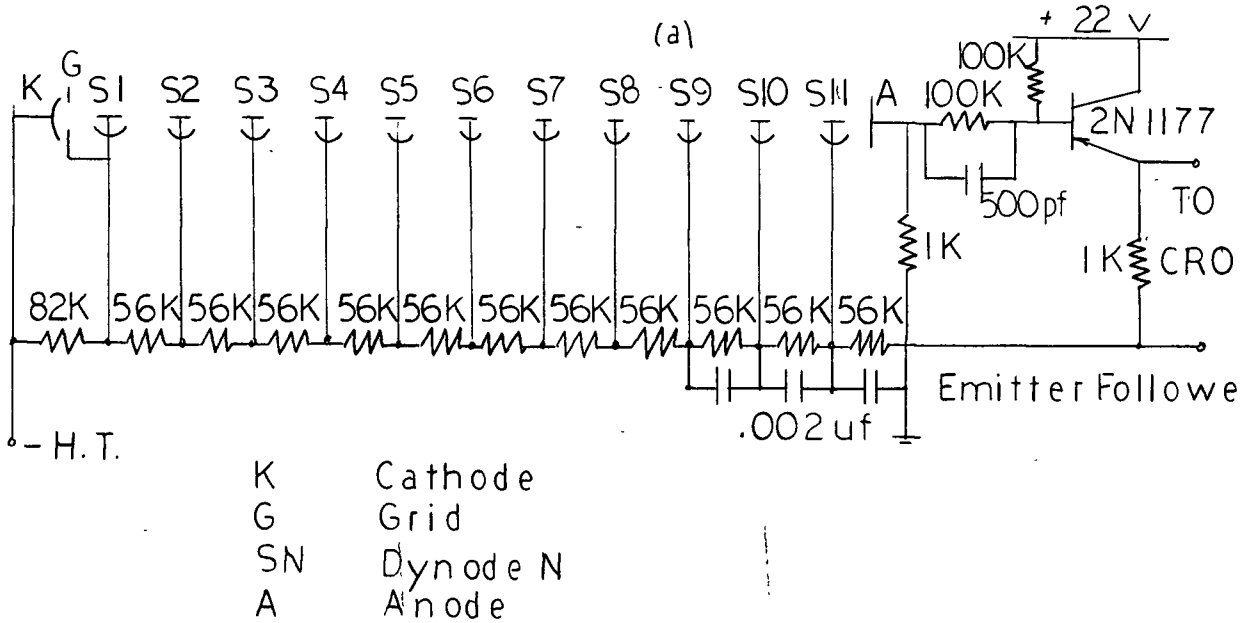


**Fig. 15: (a) Photomultiplier (EMI 9558B) circuitry**
**(b) Linear Response of Photomultiplier**

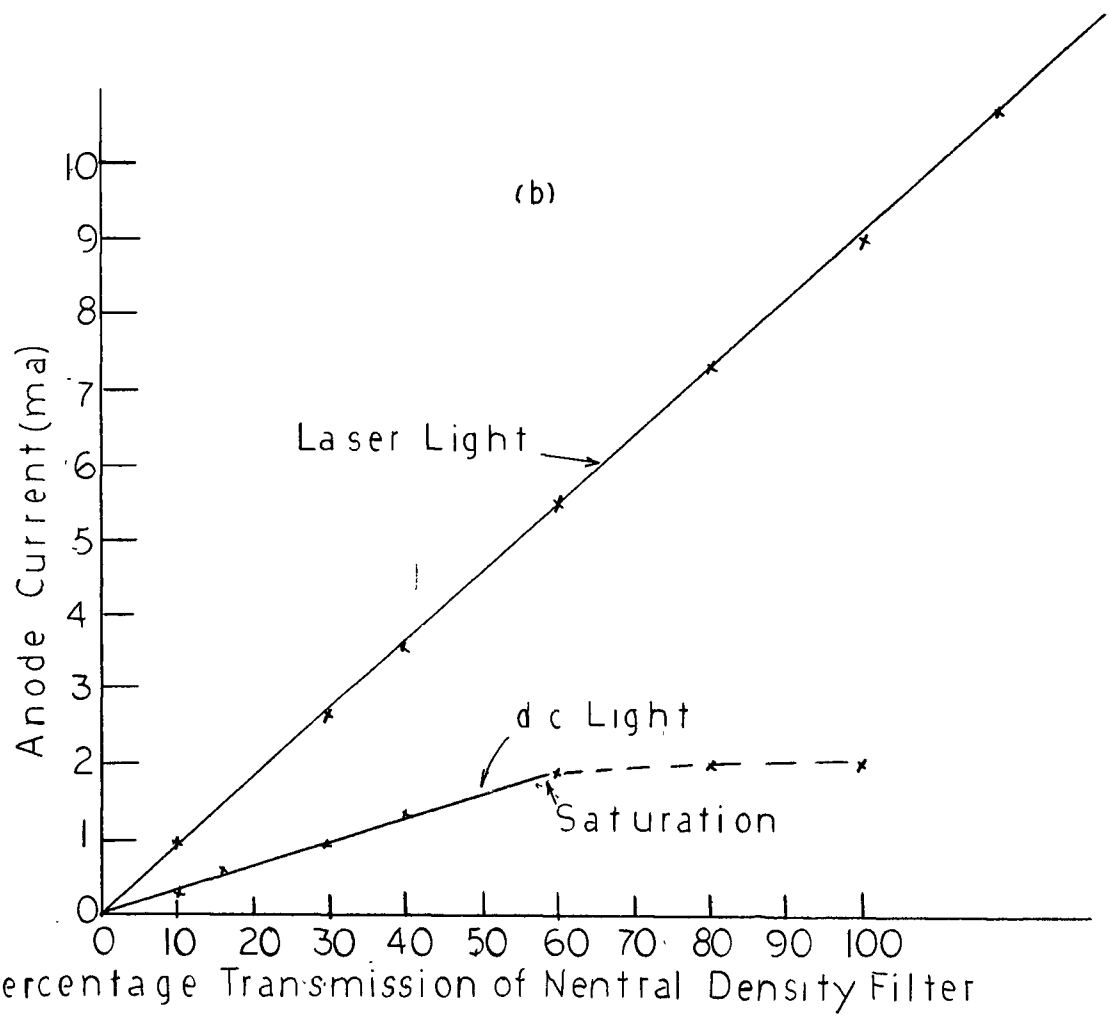

| | |
|---|---|
| Gas used | Argon |
| Rate of Gas Flow | 15 m $sec^{-1}$ |
| Pressure | Atmospheric |
| Voltage between Anode and Cathode | 15 volts |
| Current of Jet | 250,280,300 amps. |
| Observation angle | $45^{o}$ |
| Solid angle | 0.01 steradian |
| Bandpass of Monochromator slit | 8Å (500 μ slit) |

(i) CVP 150 Photomultiplier Work

Fig. 16 shows some typical oscilloscope traces at several wavelengths. It is seen that the signal-to-noise ratio is about unity and we found it necessary to use a sampling technique. At each of the 14 selected monochromator settings, 10 shots were taken and the oscilloscope traces of the photomultiplier output and photodiode were photographed. The wavelength settings for successive shots were selected at random (using random number table) to eliminate possibility of drift effects in the plasma or in the instruments influencing the average result at any particular wavelength. The size of the photomultiplier signal for each of the shots was measured from the oscillograms at seven points along the time axis near the time occurrence of the laser pulse and the ten readings were averaged. The accuracy of this method is limited by the fineness of the oscilloscope traces and by the number of the traces taken.

Fig. 17 shows some averaged traces.There is a good signal 6910 Å but not one at 6890 Å. The relative intensity of the scattered radiation as a function of wavelength shift is plotted in Fig. 18, where the vertical bars represent the standard

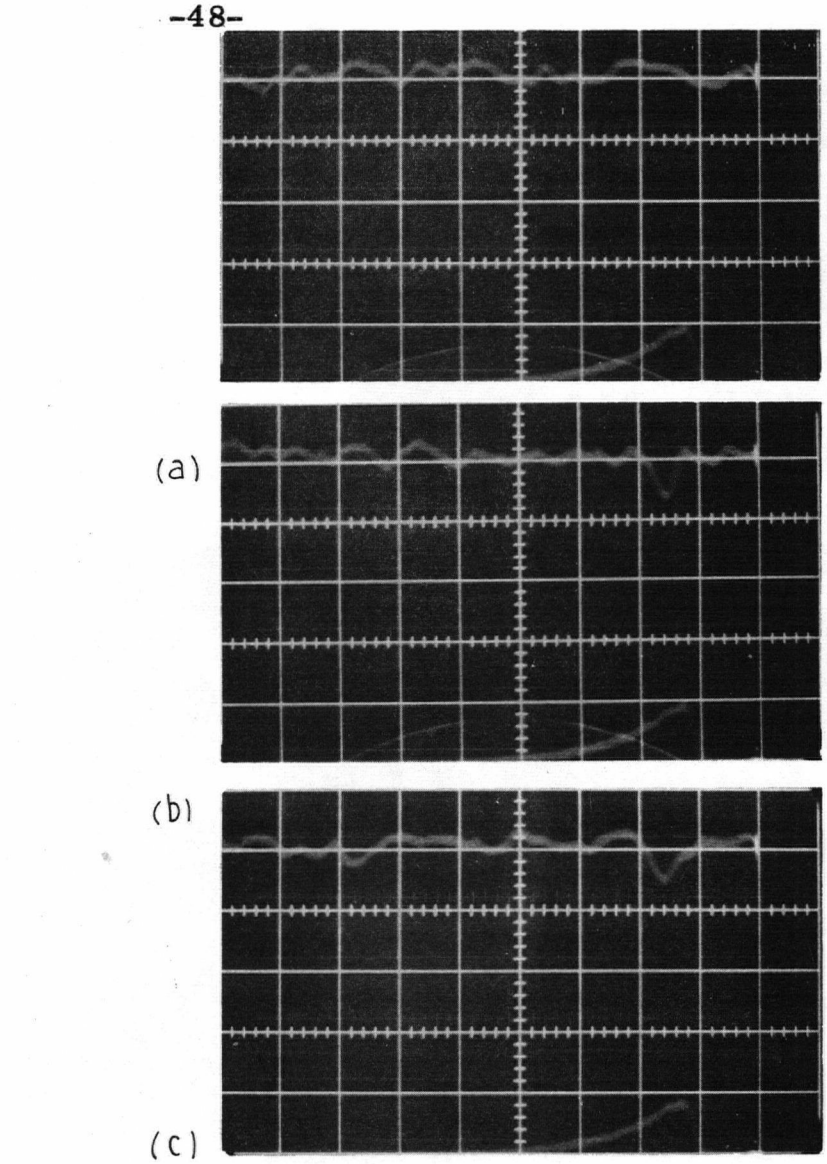


Fig. 16: Oscilloscope Traces of Scattered Signal (Plasma Jet)
(a) $\lambda$ = 7016Å
(b) $\lambda$ = 6910Å
(c) $\lambda$ = 6986Å
Upper trace: Photomultiplier signal (CVP 150)
Lower trace: Photo-diode Monitor Signal (long decay time is due to loading by cable)
Time scale: 0.1 μs/cm
Voltage scale: 0.1 v/cm (upper trace)
2 v/cm (lower trace)
Plasma Current = 280 amps.

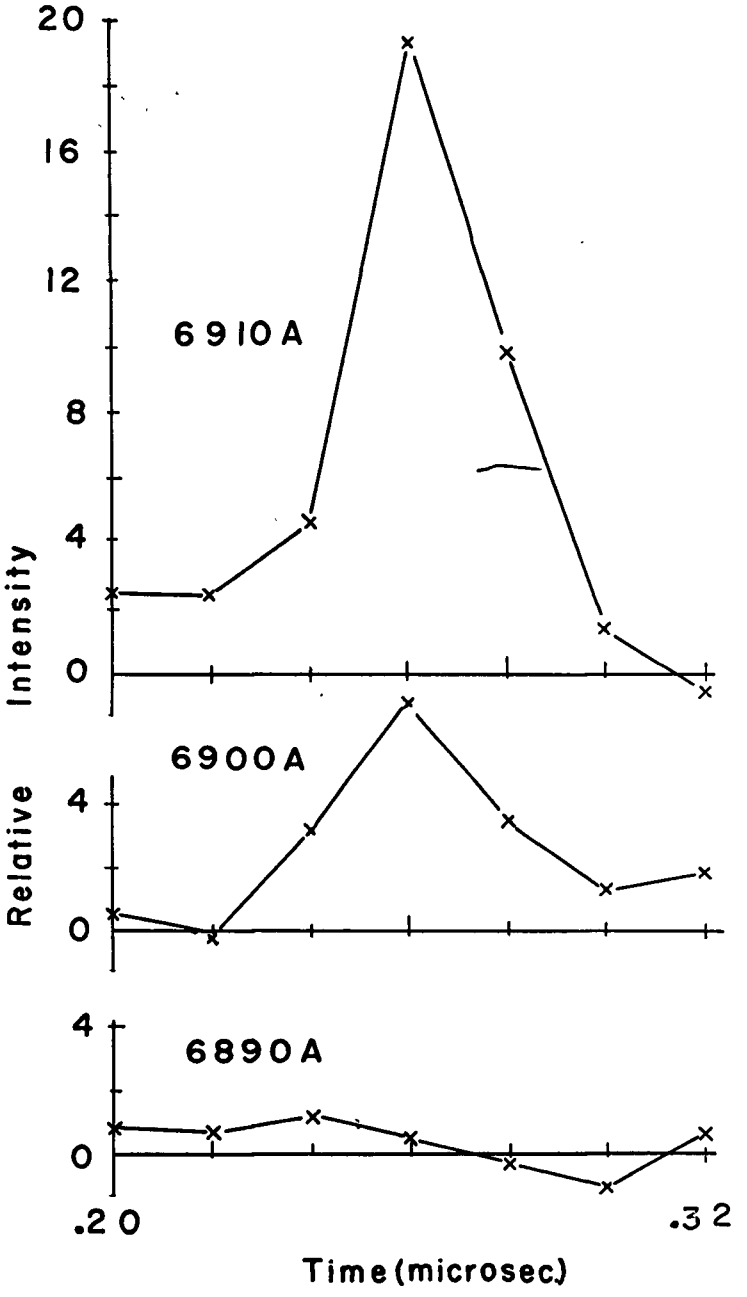


Fig. 17: Averaged traces of 10 scope traces, indicating a clear signal at 6910Å. The laser pulse occurs at 0.26 μ sec.

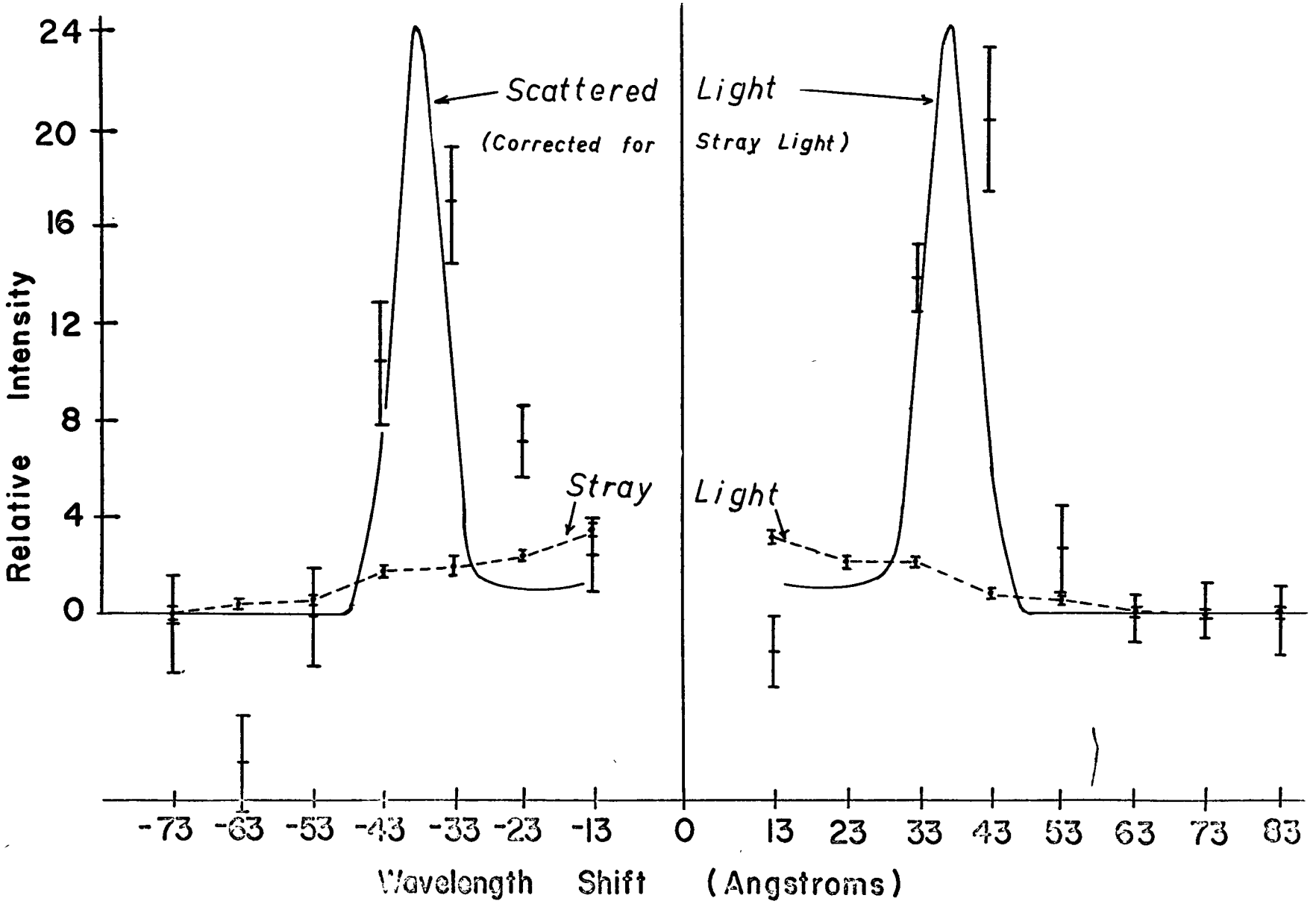


Fig. 18: Scattered Light Spectrum from Plasma Jet.
Also shown is the theoretical curve for $T_e = 13,500^{\circ}K$, an $\alpha = 4.4$, an instrumental width of 8Å, and an intensity chosen arbitrarily

deviation of the mean for the ten experimental points. The satellites occur at ± 38 Å from the central line and has a half-width of about 12 Å to 14 Å. The experimental point at + 23 Å is purposely omitted because the argon at 6965 A saturates the photomultiplier making it impossible to obtain a signal.

An interesting effect is the negative signal at -63 Å. It has been checked that this is not due to instrumental effect. However we note that there is an argon line at about 6880 Å and we interpret the decrease in the light output as due to the depopulation of the upper state of the line. This decrease amounts to about 5% of the d.c.light level. The same effect is observed in a later check at 6965 Å.

We attempted a least square fit of the theoretical curve to the experimental points but were unable to obtain a good fit because the observed linewidths are wider than those predicted by theory. The discrepancy may be accounted for by a variation of the electron density in the plasma volume we observed. According to Ahlborn[25], the temperature changes from 13,500°K to 11,500°K in a distance of 1 mm from the center of the jet. If we assume local thermal equilibrium, then according to the curves shown in Fig. 19[26], the electron density changes from about $10^{17}$ to $5\times10^{16}$ $cm^{-3}$. Assuming $\alpha$ is large, and using the relation $\omega_0^2 = \omega_{pe}^2 + \frac{3k^2 kT_e}{m_e}$, for $\theta = 45°$, $k = 2K \sin \theta/2 = 0.67\times10^5$ $cm^{-1}$, it can be calculated that the difference in the frequency shifts for the two electron densities is $\Delta\omega = 5.1\times10^{12}$ rad. $sec^{-1}$ giving a $\Delta\lambda$ of 12 Å, agreeing well with the width of the observed satellites. Of course temporal changes in $n_e$ would lead to similar results

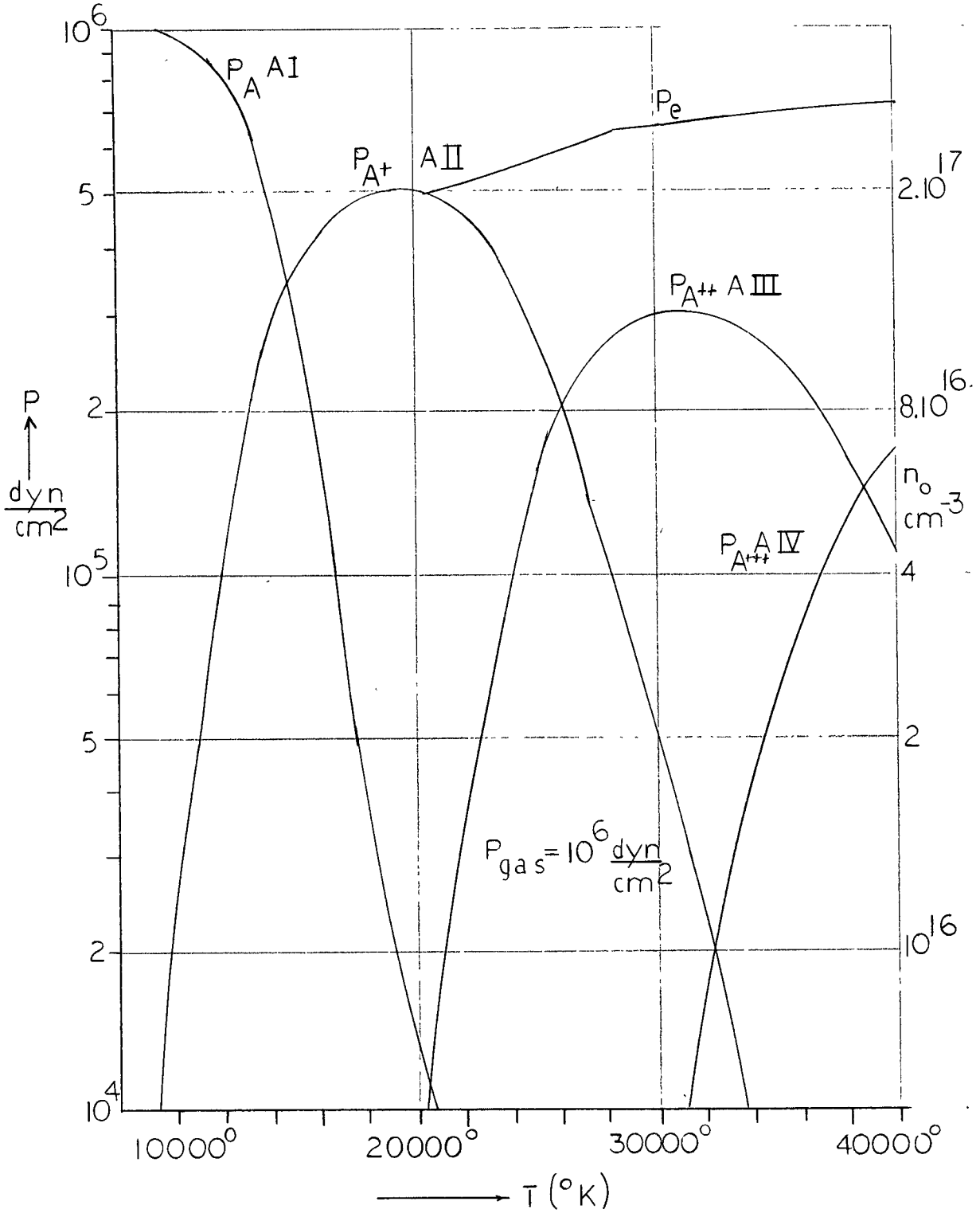


Fig. 19: Equilibrium Compositions of Argon Plasma

but this experiment does not distinguish which variation is occurring. Recently Nyugen-Quang-Dong[27] suggested that this broadening may also be accounted for by collision. Also the intensity of the line drops by a factor of half at such shifted frequency as it should because of the drop in $n_e$.

Since we cannot get a good fit, we cannot determine $n_e$ and $T_e$. However by taking Ahlborn'value of 13,500°K for the temperature at the center of the jet, the theoretical curve whose peaks coincide with the experimental peaks is obtained with $\alpha = 4.4$. This value of $\alpha$ leads to an electron density of $6.5 \times 10^{16}$ $cm^{-3}$, agreeing well with the local thermal equilibrium assumption.

Scattering from the central peak at the laser frequency is also observed. This signal is larger than that observed at the satellites by a factor of more than 20 as it should be since theory requires that its intensity is $\alpha^2$ times the intensity of each satellite. However the stray light at the center is also large primarily due to the presence of dust particles. Fig. 20a shows the laser light as a function of plasma current. If the jet is run at a low current of 50 amps.( which is the lowest value conveniently reached with the present power supply), the stray light is reduced by a great factor than when no plasma is present. This is interpreted to be due to the fact that the plasma is cleaning up the dust particles. The scattered light at the central frequency is determined as follows. The current in the jet is set at 50 amps. at which the scattered light from the electrons may be neglected, and therefore the light signal observed is equal to stray light. This value is subtracted from

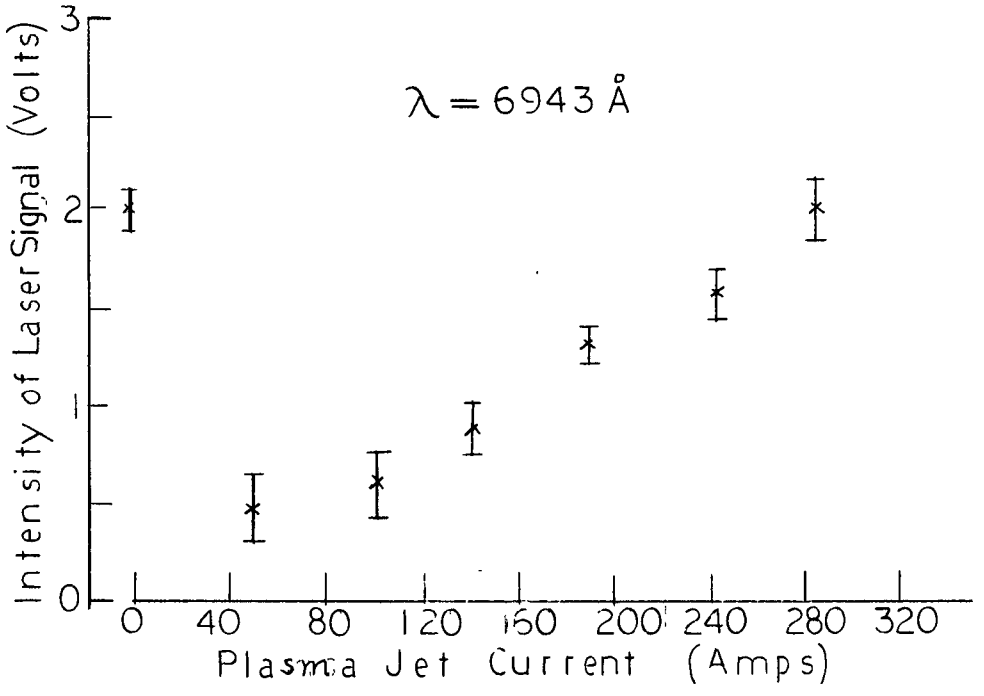


Fig. 20: (a) Intensity of Laser Light as a function of plasma current

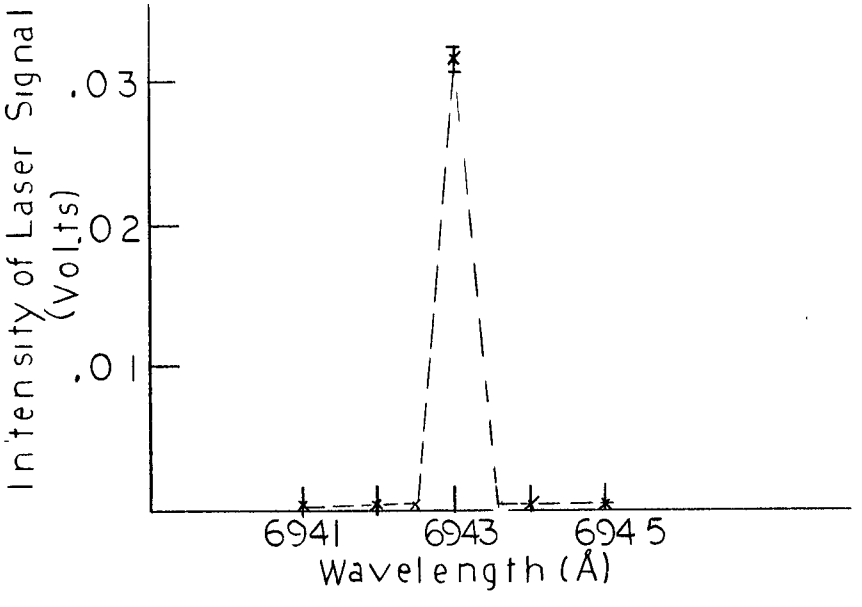


Fig. 20: (b) Scattered Spectrum of Central Peak (λ= 6943Å), using slit of 1/2Å passband

the signal obtained at 280 amps. to give the scattered signal at the central frequency. The width of the central peak is found to be narrower than $\frac{1}{2}$ Å (Fig. 20b). Better resolution cannot be obtained with the present apparatus.

(ii) EMI 9558B Photomultiplier Work

Subsequent experiments with the EMI 9558B tube have confirmed and improved on the work of the Philips CVP 150 tube. A typical oscilloscope trace is shown in Fig.21 and a signal-to-noise ratio of about 2 or 3 is obtained at the satellites so taht we can pick out the signal without the sampling required previously.

Because of slightly different electrode conditions, the parameters have changed a little so that the results may not be compared directly with the results obtained with the CVP 150 tube(i). Two experiments were done, one at 300 amps. and the other at 250 amps., and the scattered intensities are shown in Fig. 22 and in Fig. 23 respectively. The peaks occur at $\pm$ 50 Å and at $\pm$ 42 Å corresponding to an $n_e$ of $1.1 \times 10^{17}$ $cm^{-3}$ and $7.5 \times 10^{16}$ $cm^{-3}$ respectively if $T_e$=13,500°K. The widths of the satellite lines are approximately 12 Å at 300 amps. and 15 Å at 250 amps. These results cannot be very accurate because of the 8 Å bandpass of the monochromator slit.The intensity of the central peak at the laser frequency is again more than 20 times greater than that of the satellite. The line shape of this central peak has not been investigated further due to the present limitation of the optical resolution of the apparatus. We have used a slit of 25 $\mu$ wide($\frac{1}{2}$Å bandpass) to look at the central peak, and found that the central line is at most $\frac{1}{2}$Å wide, so that we are probably measuring the instrumental width.

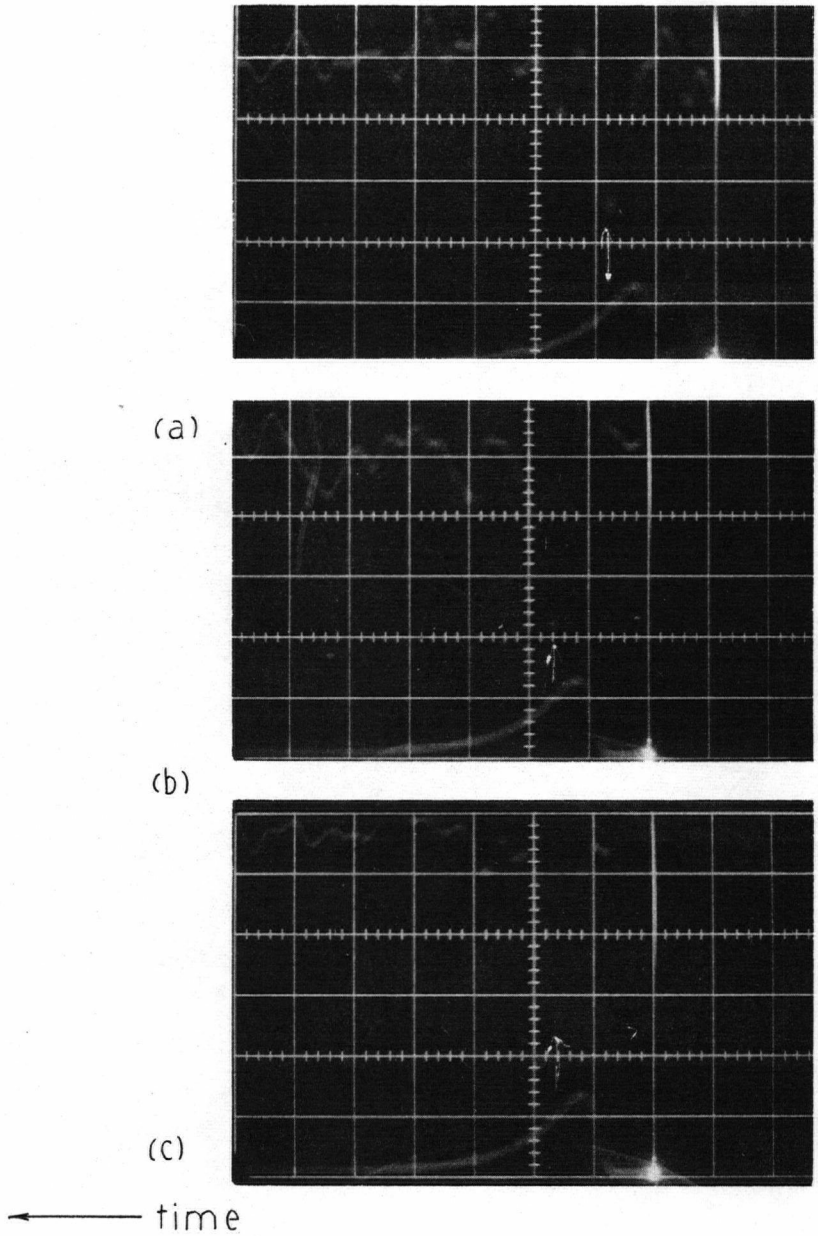


Fig. 21: Oscilloscope traces of Scattered Signal (Plasma Jet)

(a) $\lambda$ = 6900Å
(b) $\lambda$ = 6910Å
(c) $\lambda$ = 6986Å
Upper Trace: Photomultiplier Signal EMI 9558B
Lower Trace: Photo-diode Monitor
Time Scale: 0.1 μs/cm
Voltage Scale: .05 v/cm
Plasma Current: 250 amps.

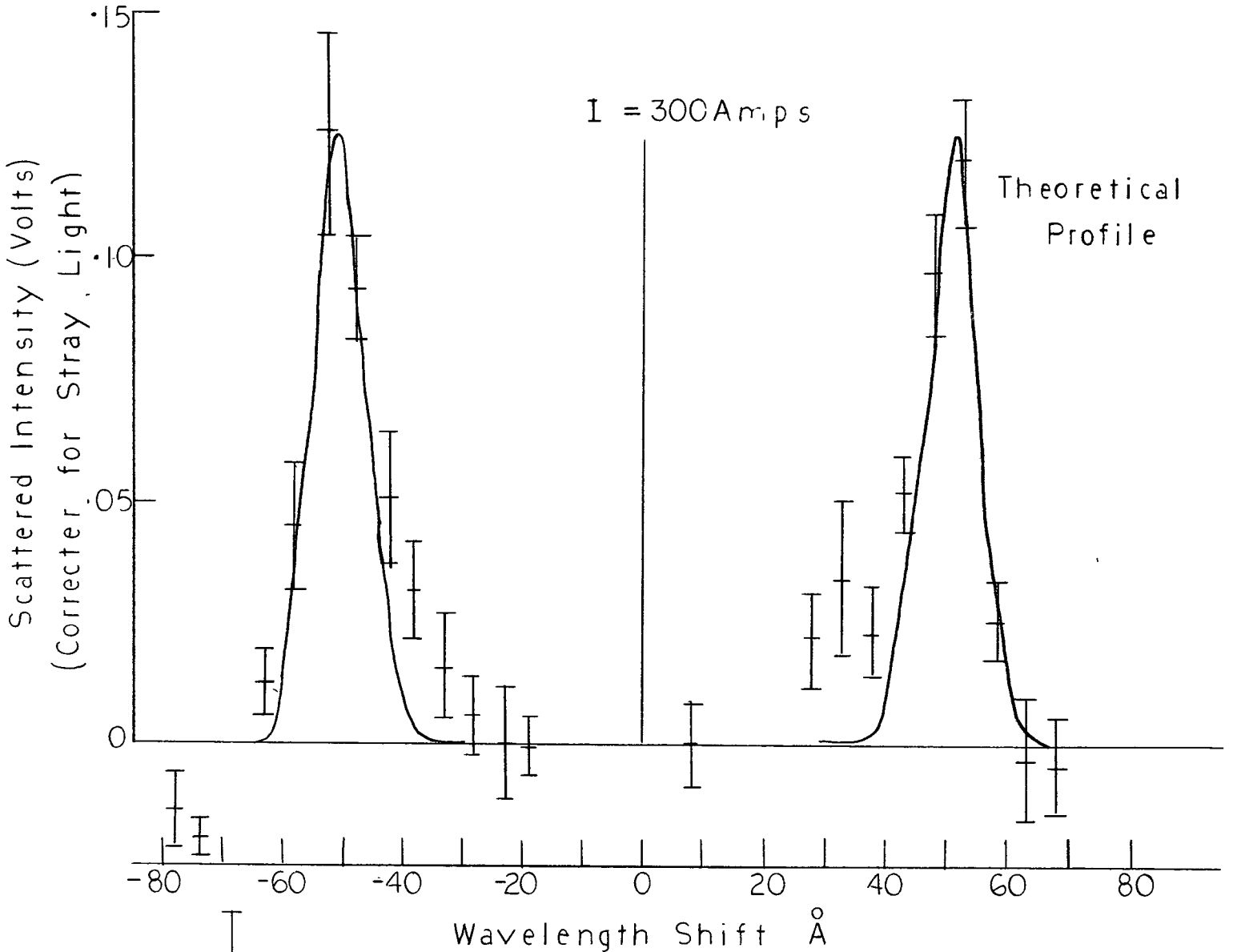


Fig. 22: Scattered Spectrum of Laser Light by Plasma Jet at 300 amps.

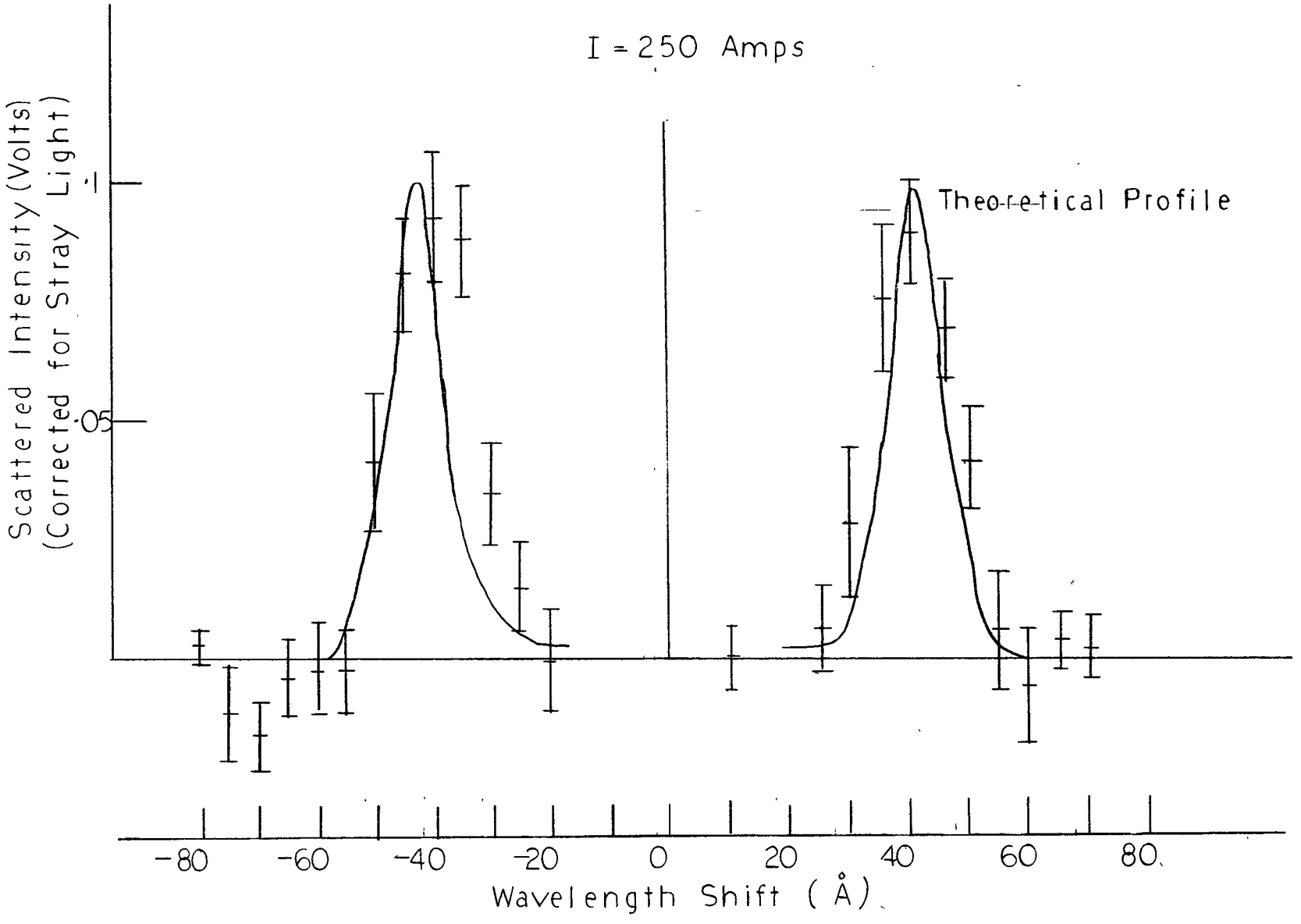


Fig. 23: Scattered Spectrum of Laser Light by Plasma Jet at 250 amps.

## CHAPTER VI CONCLUSION

The scattering method has been successfully applied both to the verification of the theory of scattering of electromagnetic waves by plasmas and to the determination of plasma parameters. Theoretical predictions have been confirmed by experimental results. For the case of scattering from the θ-pinch plasma at $90^o$, where $\alpha$ is expected to be small, the scattered spectrum shows a nearly Gaussian shape corresponding to non-collective scattering from electrons. The electron temperature is determined to be $T_e = 25{,}000^oK \pm 6{,}000^oK$ and the electron density to be $n_e = (1.0 \pm 0.3) \times 10^{16}\ cm^{-3}$ for an $\alpha = 0.60 \pm 0.21$. For the case of scattering from the plasma jet at $45^o$ where $\alpha$ is expected to be large, distinct satellite peaks were observed on both sides of the central frequency, indicating a strong collect scattering effect. By assuming the electron temperature of the jet to be $13{,}500^oK$ ( according to Ahlborn), an $\alpha$ of 4.4 is obtained for the experimental points, giving an $n_e$ of $6.5 \times 10^{16}\ cm^{-3}$. The positions and intensities of the satellites are found to vary in an expected manner with the plasma current. The intensity of the central peak is at least 20 times the intensity of each satellite, again agreeing well with theoretical prediction. Some indications of perturbation of the plasma by the laser were observed. The perturbation, though small in the present case, may become significant if a more powerful laser is used.

A few comments of the scattering method as a diagnostic technique for laboratory plasmas are in order. The method is unique amongst other diagnostic methods in that it is able to

give both very good time and spatial resolution. The method offers several difficulties of its own. Firstly because such a small fraction of light is scattered that even for plasmas of moderate densities, the scattered radiation is small enough to pose detection problem. Secondly stray light is very troublesome and elaborate light baffling has to be undertaken. As we have noted, a small variation of electron density will broaden the widths of the satellite peaks, so that observation should be made over a volume of plasma in which the density is uniform if precise plasma parameters are to be determined.

Future work will certainly include a more detailed study of the electron satelline peaks as a function of experimental parameters such as by varying $T_e$ or $n_e$ or by using different gases, gas flows, scattering angles and a detailed investigation of the centrak peak. The experiment on the central peak will involve high optical resolution techniques such as the Fabry-Perot interferometer. Hydrogen or helium is preferable because the central peak will be expected to be wider. The stray light from the laser has to be furthered reduced, for example, by building a dust-free chamber around the jet so that a better scattered light to stray light ratio may be obtained. More detailed studies should also be made on the perturbation effect of the laser on the plasma.

## APPENDIX

### A. Calculation of $\langle |\hat{n}_e(k,\omega)|^2 \rangle$

Assume that a particle of species i moves in an assigned orbit through a plasma consisting of electrons and ions that is described by the Vlasov Equations. The equations to be solved are

$$\left(\frac{\partial}{\partial t} + \underline{v}\cdot\frac{\partial}{\partial \underline{r}}\right)\delta f_{ij}(\underline{r},\underline{v},t) = \frac{q_i}{m_j}\nabla\phi_{eff}\cdot\frac{\partial f_j(\underline{v})}{\partial \underline{v}} \qquad (1)$$

$$\nabla^2\phi_{eff} = -4\pi q_i\,\delta(\underline{r}-\underline{r}_0-\underline{v}_1 t) - 4\pi n_0\sum_j \delta f_{ij}(\underline{r},\underline{v},t)\,d\underline{v} \qquad (2)$$

where

$$f_j(\underline{v}) = \left(\frac{m_j}{2\pi k T_j}\right)^{3/2}\exp\left(-\frac{m_j v^2}{2kT_j}\right) \qquad (3)$$

is the unperturbed field-particle distribution function (normalised to unity) which is assumed to be stationary and spatially homogeneous. $\delta f_{ij}(\underline{r},\underline{v},t)$ is the change in the distributing function of the field particles of species j produced by the test particles i at $\underline{r}_1 = \underline{r}_0 + \underline{v}_1 t$,

$\phi_{eff}$ is the effective electric potential

$n_0$ is the average number density of electrons at thermal equilibrium qj,mj are the charge and mass of the particle of species j respectively. The time-asymptotic solution of this problem has been solved by Rostokor & Rosenbluth and also given in standard texts.[2,8] The method is to Fourier analyse Equation (1) & (2) both in space and time by the following transforms.

$$\delta f_{ij}(\underline{r},\underline{v},t) = \frac{1}{(2\pi)^3}\int d\underline{k}\, e^{i\underline{k}\cdot\underline{r}}\,\delta\hat{f}_{ij}(\underline{k},\underline{v},t) \qquad (4)$$

$$\delta\hat{f}_{ij}(\underline{k},\underline{v},t) = \frac{1}{2\pi}\int dz\, e^{-izt}\,\delta\hat{\hat{f}}_{ij}(\underline{k},\underline{v},z) \qquad (5)$$

The final results are

$$\delta f_{ij}(\underline{r},\underline{v}) = \frac{4\pi q_i q_j}{m_j}\int\frac{d\underline{k}}{(2\pi)^3}\,\frac{e^{i\underline{k}\cdot(\underline{r}-\underline{r}_1)}\;\underline{k}\cdot\frac{\partial f_j}{\partial \underline{v}}}{k^2\,\epsilon(\underline{k},-\underline{k}\cdot\underline{v}_1)[\underline{k}\cdot(\underline{v}-\underline{v}_1)-i\lambda]} \qquad (6)$$

where

$$\epsilon(\underline{k},-\underline{k}\cdot\underline{v}_1) = 1 - \sum_j\frac{\omega_{pj}^2}{k^2}\int\frac{\left(\underline{k}\cdot\frac{\partial f_j}{\partial \underline{v}}\right)d\underline{v}}{\underline{k}\cdot(\underline{v}-\underline{v}_1-i\lambda)} \qquad \lambda\to 0 \qquad (7)$$

$$\omega_{pj}^2 = \frac{4\pi n_0 Z e^2}{m_j} \tag{8}$$

The electron distribution in the neighbourhood of a test particle can now be calculated. If the test particle is an electron, with position and velosity $(\underline{r}_e, \underline{v}_e)$, then the electron number density at $(\underline{r}, t)$ when a test particle is at $r_e$ and $v_e$ $(t=0)$ is

$$n_e(\underline{r},t \mid \underline{r}_e, \underline{v}_e) = \delta(\underline{r}-\underline{r}_e) + n_0 \int d\underline{v}\,[f_e(\underline{v}) + \delta f_{ee}(\underline{r},\underline{v})]$$

$$= n_0 + \int \frac{d\underline{k}}{(2\pi)^3}\, e^{i\underline{k}\cdot(\underline{r}-\underline{r}_e-\underline{v}_e t)} \left[1 + \frac{\omega_{pe}^2}{k^2\epsilon(\underline{k})} \int \frac{d\underline{r}\;\underline{k}\cdot\frac{\partial f_e(\underline{v})}{\partial \underline{v}}}{\underline{k}\cdot(\underline{v}-\underline{v}_e)-i\lambda}\right. \tag{9}$$

and similarly for an ion test particle with position and velocity given by $(\underline{r}_I, \underline{v}_I)$

$$n_e(\underline{r},t \mid \underline{r}_I, \underline{v}_I) = n_0 \int d\underline{v}\;[f_e(\underline{v}) + \delta f_{Ie}(\underline{r},\underline{v})$$

$$= n_0 - \int \frac{d\underline{k}}{(2\pi)^3}\, e^{i\underline{k}\cdot(\underline{r}-\underline{r}_I-\underline{v}_I t)} \frac{\omega_{pe}^2}{k^2\epsilon(\underline{k})} \int d\underline{r}\; \frac{\underline{k}\cdot\frac{\partial f_e(\underline{v})}{\partial \underline{v}}}{\underline{k}\cdot(\underline{v}-\underline{v}_I)-i\lambda} \tag{10}$$

To simplify (9) and (10), the following substitutions are made

$$u \equiv \underline{k}\cdot\underline{v}/k \tag{11}$$

$$F_e(u) = \int d\underline{v}\, f_e(\underline{v})\, \delta(u - \underline{k}\cdot\underline{v}/k)$$

$$= \int d\underline{v}\, f_e(\underline{v})\, \delta(u - v_z)$$

$$= \int dv_x\, dv_y \int_{-\infty}^{\infty} dv_z\, f_e(\underline{v})\, \delta[u - v_z]$$

$$= \int dv_x\, dv_y\; f_e(v_x, v_y, u)$$

$$= \left(\frac{m_e}{2\pi k T_e}\right)^{3/2} e^{-m_e u^2/2kT_e} \iint dv_x\, dv_y\, e^{-m_e(v_x^2+v_y^2)/2kT_e}$$

$$\therefore\; F_e(u) = \left(\frac{m_e}{2\pi k T_e}\right)^{1/2} e^{-m_e u^2/2kT_e} \tag{12}$$

$$\therefore \int \frac{du}{u-u_j-i\lambda} F_e'(u) = \int \frac{du}{u-u_j-i\lambda} \int d\underline{v}\, \frac{\underline{k}}{k}\, \frac{\partial f_e(\underline{v})}{\partial \underline{v}}\, \delta\left(u - \frac{\underline{k}\cdot\underline{v}}{k}\right) \tag{13}$$

$$= \int \frac{d\underline{v}\;\; \underline{k}\cdot\frac{\partial f_e(\underline{v})}{\partial(\underline{v})}}{\underline{k}\cdot(\underline{v}-\underline{v}_j)-i\lambda}$$

$$\epsilon(\underline{k}) \equiv \epsilon(u) = 1 - \sum_j \frac{\omega_{pj}^2}{k^2} \int \frac{F_e'(u')}{u'-u-i\lambda}\, du' \tag{14}$$

Hence (9) & (10) become

$$n_e(\underline{r},t \mid \underline{r}_e, \underline{v}_e) = n_0 + \int \frac{d\underline{k}}{(2\pi)^3}\, e^{i\underline{k}\cdot(\underline{r}-\underline{r}_e-\underline{v}_e t)} \left[1 + \frac{\omega_{pe}^2}{k^2\epsilon(u)} \int \frac{du'}{u'-u_e-i\lambda} F_e'(u')\right] \tag{15}$$

$$n_e(\underline{r},t\,|\,\underline{r}_I,\underline{v}_I)=n_0-\int\frac{d\underline{k}}{(2\pi)^3}e^{i\underline{k}\cdot(\underline{r}-\underline{r}_I-\underline{v}_I t)}\frac{\omega_{pe}^2}{k^2\epsilon(u)}\int\frac{du'}{u'-u_I-i\lambda}F_e'(u') \quad (16)$$

Then $\langle[n_e(\underline{r},t)-n_0][n_e(\underline{r}',t')-n_0]\rangle$ (17)

$$=\sum_j\frac{n_0}{V}\int d\underline{r}_j\,d\underline{v}_j[n_e(\underline{r},t\,|\,\underline{r}_j,\underline{v}_j)-n_0][n_e(\underline{r}',t'\,|\,\underline{r}_j+\underline{v}_j(t'-t),\underline{v}_j)-n_0]f_j(\underline{v}_j)$$

$$=\frac{n_0}{V}\Big[\int d\underline{r}_e\,d\underline{v}_e[n_e(\underline{r},t\,|\,\underline{r}_e,\underline{v}_e)-n_0][n_e(\underline{r}',t'\,|\,\underline{r}_e+\underline{v}_e(t'-t),\underline{v}_e)-n_0]f_e(\underline{v}_e)$$
$$+\int d\underline{r}_I\,d\underline{v}_I[n_e(\underline{r},t\,|\,\underline{r}_I,\underline{v}_I)-n_0][n_e(\underline{r}',t'\,|\,\underline{r}_I'+\underline{v}_I(t'-t),\underline{v}_I)-n_0]f_I(\underline{v}_I)$$

Now $C(\rho,\tau)=\langle n_e(\underline{r},t)\,n_e(\underline{r}+\rho,t+\tau)\rangle/n_0$ (18)

$$=\frac{\langle[n_e(\underline{r},t)-n_0][n_e(\underline{r}+\rho,t+\tau)-n_0]\rangle}{n_0}+n_0$$

One gets $C(\rho,\tau)=n_0+\frac{1}{V}\int d\underline{r}_e\,d\underline{v}_e f_e(\underline{v}_e)\int\frac{d\underline{k}}{(2\pi)^3}e^{i\underline{k}\cdot[\underline{r}-\underline{r}_e-\underline{v}_e t]}\cdot$ (19)

$$\left[1+\frac{\omega_{pe}^2}{k^2\epsilon(u)}\int\frac{du'}{u'-u_e-i\lambda}F_e'(u')\right]\cdot\int\frac{d\underline{k}'}{(2\pi)^3}e^{i\underline{k}'\cdot[\underline{r}+\rho-\underline{r}_e-\underline{v}_e(t+\tau)]}\left[1+\frac{\omega_{pe}^2}{k'^2\epsilon(u)}\int\frac{du'}{u'-u_e-i\lambda}F_e'(u')\right]$$
$$+\frac{1}{V}\int d\underline{r}_I\,d\underline{v}_I f_I(\underline{v}_I)\int\frac{d\underline{k}}{(2\pi)^3}e^{i\underline{k}\cdot[\underline{r}-\underline{r}_I-\underline{v}_I t]}\cdot\frac{\omega_{pe}^2}{k^2\epsilon(u)}\int\frac{du'}{u'-u_I-i\lambda}F_e'(u')$$
$$\cdot\int\frac{d\underline{k}'}{(2\pi)^3}e^{i\underline{k}'\cdot[\underline{r}+\rho-\underline{r}_I+\underline{v}_I(t+\tau)}\cdot\frac{\omega_{pe}^2}{k^2\epsilon(u)}\int\frac{du'}{u'-u_I-i\lambda}F_e'(u')$$

Using

$$\frac{1}{V(2\pi)^3}\int d\underline{r}\,e^{i(\underline{k}+\underline{k}')\cdot\underline{r}}=\delta(\underline{k}+\underline{k}') \quad (20)$$

We get $C(\rho,\tau)=n_0+\int d\underline{v}_e f_e(\underline{v}_e)\int\frac{d\underline{k}}{(2\pi)^3}e^{i\underline{k}\cdot[\rho-\underline{v}_e\tau]}\left|1+\frac{\omega_{pe}^2}{k^2\epsilon(u)}\int\frac{du'}{u'-u_e-i\lambda}F_e'(u')\right|^2$

$$+\int d\underline{v}_I f_I(\underline{v}_I)\int\frac{d\underline{k}}{(2\pi)^3}e^{i\underline{k}\cdot[\rho-\underline{v}_I\tau]}\left|\frac{\omega_{pe}^2}{k^2\epsilon(u)}\int\frac{du'}{u'-u_I-i\lambda}F_e'(u')\right|^2 \quad (21)$$

Apply Fourier transform $\int\frac{d\tau}{2\pi}e^{iz\tau}$ and letting

$$\int d\underline{v}_j f_j(\underline{v}_j)\delta(z-\underline{k}\cdot\underline{v}_j)=\frac{1}{k}F_j\left(\frac{z}{k}\right) \quad \text{as before} \quad (22)$$

One gets $C(\rho,\tau)=\int_{-\infty}^{\infty}\frac{dz}{2\pi}e^{iz\tau}\Big\{2\pi n_0\delta(z)+\frac{1}{k}\int\frac{d\underline{k}}{(2\pi)^3}e^{i\underline{k}\cdot\rho}\cdot 2\pi\Big\}\cdot$

$$\cdot\Big[F_e\left(\frac{z}{k}\right)\left|1+\frac{\omega_{pe}^2}{k^2\epsilon(u)}\int\frac{du'}{u'-u-i\lambda}F_e'(u')\right|^2 \quad (23)$$
$$+F_I\left(\frac{z}{k}\right)\left|\frac{\omega_{pe}^2}{k^2\epsilon(u)}\int\frac{du'}{u'-u-i\lambda}F_e'(u')\right|^2$$

$$=\frac{1}{n_0}\int_{-\infty}^{\infty}\frac{dz}{2\pi}e^{iz\tau}\int\frac{d\underline{k}}{(2\pi)^3}\langle|\hat{n}_e(\underline{k},z)|^2\rangle$$

where

$$\langle|\hat{n}_e(\underline{k},z)|^2\rangle=(2\pi)^4 n_0\delta(z)\delta(\underline{k})+\frac{2\pi}{k}\Big[F_e\left(\frac{z}{k}\right)\left|1+\frac{\omega_{pe}^2}{k^2\epsilon(u)}\int\frac{du'}{u'-u-i\lambda}F_e'(u')\right|^2 \quad (24)$$
$$+F_I\left(\frac{z}{k}\right)\left|\frac{\omega_{pe}^2}{k^2\epsilon(u)}\int\frac{du'}{u'-u-i\lambda}F_e'(u')\right|^2$$

We see that the first term is zero except when $z=\omega=0$, $\underline{k}=0$

This is a wave with the same frequency and wave vector as the incident wave, therefore is a transmitted beam and does not

contribute to the scattered spectrum and shall be omitted from hereafter.

If we put $z = \omega$, $u = z/k$

$$\therefore \quad \langle |\hat{n}_e(k,\omega)|^2 \rangle = \frac{2\pi}{k}\left\{ \frac{F_e(u)}{|\epsilon(\omega)|^2} \left| |\epsilon(\omega)|^2 + \frac{\omega_{pe}^2}{k^2}\int \frac{du'}{u'-u-i\lambda} F_e'(u') \right|^2 \right. \tag{25}$$

$$\left. + \frac{F_I(u)}{|\epsilon(\omega)|^2} \left| \frac{\omega_{pe}^2}{k^2}\int \frac{du'}{u'-u-i\lambda} F_e'(u') \right|^2 \right.$$

Since

$$\epsilon(u) = 1 - \frac{\omega_{pe}^2}{k^2}\int \frac{du'}{u'-u-i\lambda} F_e'(u') - \frac{\omega_{pI}^2}{k^2}\int \frac{du'}{u'-u-i\lambda} F_I(u') \tag{26}$$

$$\therefore \langle |\hat{n}_e(k,\omega)|^2 \rangle = \frac{2\pi}{k}\left\{ \frac{F_e(u)}{|\epsilon(\omega)|^2}\left| 1 - \frac{\omega_{pI}^2}{k^2}\int \frac{du'}{u'-u-i\lambda} F_I(u') \right|^2 + \frac{F_I(u)}{|\epsilon(\omega)|^2}\left| \frac{\omega_{pe}^2}{k^2}\int \frac{du'}{u'-u-i\lambda} F_e'(u') \right| \right\}$$

as given by Rosenbluth & Rostoker.[4]

The simplication of (26) hinges on the calculation of the integral

$$\lim_{\lambda \to 0} \int \frac{du'}{u'-u-i\lambda} F'(u') = \fint_{-\infty}^{\infty} \frac{du'}{u'-u} F'(u') + i\pi F'(u) \tag{27}$$

where $\fint$ denotes the principal part of the integral.

For an equilibrium plasma, $F(u) = \beta \pi^{-\frac{1}{2}} e^{-\beta^2 u^2}$ $\quad (\beta^2 = m/2kT)$

$$F'(u) = -2\beta^3 \pi^{-\frac{1}{2}} u\, e^{-\beta^2 u^2} = 2\beta^2 \pi^{-\frac{1}{2}} F(u)$$

Making the change $u' = u + \tau$, one can write for an equilibrium plasma

$$I(u) \equiv \fint_{-\infty}^{\infty} du' \frac{F'(u')}{u'-u} = 2\beta^3 \pi^{-\frac{1}{2}} \fint_{-\infty}^{\infty} du' \frac{u' e^{-\beta^2 u'^2}}{u'-u}$$

$$= -2\beta^3 \pi^{-\frac{1}{2}} \fint_{-\infty}^{\infty} d\tau\, (u+\tau) e^{-\beta^2 (u+\tau)^2}/\tau$$

$$= -2\beta^3 \pi^{-\frac{1}{2}} \left\{ \int_{-\infty}^{\infty} d\tau\, e^{-\beta^2 (u+\tau)^2} + u \lim_{\epsilon \to 0} \int_{-\infty}^{-\epsilon} + \int_{\epsilon}^{\infty} d\tau\, e^{-\beta^2(u^2+\tau^2+2u\tau)}/\tau \right.$$

$$= -2\beta^3 \pi^{-\frac{1}{2}} \left\{ \frac{\pi^{\frac{1}{2}}}{\beta} + u e^{-\beta^2 u^2} \int_0^{\infty} d\tau \frac{e^{-\beta^2\tau^2}}{\tau} \left[ 1 - e^{2\beta^2 u\tau} + e^{-2\beta^2 u\tau} \right] \right\}$$

$$= -2\beta^3 \pi^{-\frac{1}{2}} \left\{ \frac{\pi^{\frac{1}{2}}}{\beta} - u e^{-\beta^2 u^2}\, 2 \int_0^{\infty} d\tau\, e^{-\beta^2\tau^2} \sinh e^{-2\beta^2 u\tau}/\tau \right\}$$

Write $\beta u \equiv x = \omega/\omega_e$, $(\omega_e = [2k^2 KT_e/m_e]^{\frac{1}{2}})$, $\beta\tau = t$

$$\therefore \quad I(u) = -2\beta^3 \pi^{-\frac{1}{2}} \left\{ \frac{\pi^{\frac{1}{2}}}{\beta} - \frac{x}{\beta} e^{-x^2}\, 2 \int_0^{\infty} dt\, e^{-t^2} \frac{\sinh 2xt}{t} \right. \tag{28}$$

$$= -2\beta^3 \left\{ 1 - \pi^{\frac{1}{2}} x\, e^{-x^2}\, 2 \int_0^{\infty} dt\, e^{-t^2} \frac{\sinh 2xt}{t} \right\}$$

To evaluate $\quad I(x) \equiv \int_0^{\infty} dt\, e^{-t^2} \dfrac{\sinh 2xt}{t}$

We first differentiate and obtain

$$I'(x) = \int_0^{\infty} dt\, e^{-t^2}\, 2 \cosh 2xt \tag{29}$$

$$= \frac{2}{x} \int_0^{\infty} dt\, e^{-t^2}\, t \sinh 2xt$$

Differentiate (29) again

$$I''(x) = \int_0^\infty dt\, e^{-t^2} 2t \sinh 2xt = 2\int_0^\infty dt\, e^{-t^2}\, t.\sinh 2xt \tag{30}$$

Hence we have

$$I'(x) = \frac{1}{x}\, I''(x) \tag{31}$$

Let $\quad y = I'(x)$

$$\therefore \quad y = C\, e^{x^2}$$

where C can be obtained from (29) at $x = 0$,

$$y = \int_0^\infty 2\, dt\, e^{-t^2} = C = \pi^{\frac{1}{2}}$$

$$\therefore\ I(x) = \pi^{\frac{1}{2}} \int_0^x dt\, e^{t^2} + C' \qquad \text{where} \quad C' = 0 \tag{32}$$

$$= \pi^{\frac{1}{2}} \int_0^x dt\, e^{t^2}$$

$$\because\ I(u) = -2\beta^2 \{ 1 - 2\pi^{-\frac{1}{2}} I(x) \} \tag{28}$$

$$\therefore\ I(u) = -2\beta^2 \{ 1 - 2x\, e^{-x^2} \int_0^x e^{t^2} dt \tag{33}$$

Hence $\quad \frac{\omega_{pe}^2}{k^2} \int \frac{du'}{u'-u-i\lambda} F_e'(u')$

$$= -\frac{\omega_{pe}^2}{k^2} \left[ 2\beta_e^2 \{ 1 - 2x\, e^{-x^2} \int_0^x e^{t^2} dt \} + i\pi\beta_e^2\, 2x\, e^{-x^2} \right] \tag{34}$$

$$= -\alpha^2 \left[ 1 - 2x\, e^{-x^2} \int_0^x e^{t^2} dt + i\pi^{\frac{1}{2}}\, x\, e^{-x^2} \right]; \quad \alpha^2 = \frac{2\omega_{pe}^2 \beta_e^2}{k^2}$$

$$= -\alpha^2 \left[ 1 - f(x) + i\pi^{\frac{1}{2}}\, x e^{-x^2} \right]$$

Where $f(x)$ is defined by

$$f(x) \equiv 2x\, e^{-x^2} \int_0^x e^{t^2} dt \tag{35}$$

Similarly

$$\frac{\omega_{pI}^2}{k^2} \int \frac{du'}{u'-u-i\lambda} F_I'(u') = -\left( \frac{Z T_e \alpha^2}{T_I} \right) \left[ 1 - f(y) + i\pi^{\frac{1}{2}} y\, e^{-y^2} \right] \tag{36}$$

Where $\quad f(y) \equiv 2y\, e^{-y^2} \int_0^y e^{t^2} dt$

and $y \equiv \beta_I u = \frac{\omega}{\omega_I}$ and the ion charge $Z$ is taken into account.

Find we have

$$\langle |\hat{n}_e(k,\omega)|^2 \rangle = \frac{2\pi}{k} \frac{|1 - G_I|^2 F_e(u) + Z\, |G_e|^2 F_I(u)}{|1 - G_I - G_e|^2} \tag{37}$$

Where $\quad G_e(\omega) = -\alpha^2 [1 - f(x) + i\pi^{\frac{1}{2}} x e^{-x^2}], \quad x_e \equiv \frac{\omega}{\omega_e}, \quad \omega_e = \left( \frac{2k^2 k T_e}{m_e} \right)^{\frac{1}{2}}$

$$G_I(\omega) = -\left( \frac{Z T_e \alpha^2}{T_I} \right) [1 - f(y) + i\pi^{\frac{1}{2}}\, y\, e^{-y^2}, \quad x_I \equiv \frac{\omega}{\omega_I}, \quad \omega_I = \left( \frac{2k^2 k T_I}{m_I} \right)^{\frac{1}{2}}$$

$$f(x) = 2x\, e^{-x^2} \int_0^x e^{t^2} dt$$

$$F_e(u) = \left(\frac{m_e}{2\pi k T_e}\right)^{\frac{1}{2}} \exp\left(-\frac{m_e u^2}{2kT_e}\right)$$
$$F_I(u) = \left(\frac{m_I}{2\pi k T_I}\right)^{\frac{1}{2}} \exp\left(-\frac{m_I u^2}{2kT_I}\right)$$

in the form given by Salpeter.[2]

## B. Case of Practical Interest

We consider the case when $T_I \lesssim T_e$ so that $\eta \equiv \frac{\omega_I}{\omega_e} = \left(\frac{m_e T_I}{m_I T_e}\right)^{\frac{1}{2}} \ll 1$ In this case a good approximation can be given to the general expression given in (37).

(i) Consider the first term $\frac{|1-G_I|^2 F_e(u)}{|1-G_e-G_I|^2}$. It involves $F_e(u) = \frac{k\omega_e}{\pi^{\frac{1}{2}}} \exp(-x^2)$ and is of most interest for $|x| \sim 1$. Disregarding the narrow region $|x| = |y|\eta \lesssim \eta$ we have $|y| \gg 1$ for this term and $G_I = \frac{Z T_e \alpha^2}{2 T_I y^2}$ can be neglected compared with $G_e$ and unity.

Hence we have

$$\frac{|1-G_I|^2 F_e(u)}{|1-G_e-G_I|^2} \simeq \frac{k}{\pi^{\frac{1}{2}}\omega_e} \frac{\exp(-x^2)}{|[1+\alpha^2-\alpha^2 f(x) - i\pi^{\frac{1}{2}} x e^{-x^2}]|^2}$$
$$= \frac{k}{\pi^{\frac{1}{2}}\omega_e} \frac{\exp(-x^2)}{[1+\alpha^2-\alpha^2 f(x)]^2 + \pi\alpha^4 x^2 e^{-x^2}} \equiv \frac{k}{\pi^{\frac{1}{2}}\omega_e} \Gamma_\alpha(x)$$

Where $\Gamma_\alpha(x) \equiv \exp(-x^2)\{[1+\alpha^2-\alpha^2 f(x)]^2 + \pi\alpha^4 x^2 \exp(-2x^2)\}^{-1}$ (38)

(ii) For the second term where $F_I = \frac{k}{\pi^{\frac{1}{2}}\omega_I} e^{-y^2}$, and is unimportant if $|y| = |x|\eta^{-1} \gg \eta^{-1}$. In the important regions we then have $|x| \ll 1$ and $G_e \simeq -\alpha^2[1 - f(x) + i\pi^{\frac{1}{2}} x \exp(-x^2)] \simeq -\alpha^2$

$$\therefore \frac{Z|G_e|^2 F_I(u)}{|1-G_e-G_I|^2} \simeq \frac{k}{\pi^{\frac{1}{2}}\omega_I} \frac{Z\alpha^4 \exp(-y^2)}{[1+\alpha^2+\alpha^2(1-f(y)+i\pi^{\frac{1}{2}} y \exp(-y^2)]^2}$$
$$= Z\left(\frac{\alpha^2}{1+\alpha^2}\right)^2 \frac{\exp(-y^2)}{[1+\beta^2-\beta^2 f(y)]^2 + \pi\beta^4 y^2 \exp -y^2}$$
$$\equiv Z\left(\frac{\alpha^2}{1+\alpha^2}\right)^2 \Gamma_\beta(y)$$

Where $\Gamma_\beta(y) \equiv \exp(-y^2)\{[1+\beta^2-\beta^2 f(y)]^2 + \pi\alpha^4 y^2 \exp(-2y^2)\}^{-1}$ (39)

$\beta^2 \equiv [Z T_e \alpha^2 / T_I (1+\alpha^2)]$

$$\therefore \langle|\hat{n}_e(k,\omega)|^2\rangle d\omega \sim \Gamma_\alpha(x)\frac{d\omega}{\omega_e} + Z\left(\frac{\alpha^2}{1+\alpha^2}\right)^2 \Gamma_\beta(y)\frac{d\omega}{\omega_I} \qquad (40)$$

Equation (40) together with (38) & (39) will give the essential features of the scattered profile.

## C. Spectrum of Scattered Radiation for $\alpha \gtrsim 1$

The case for $\alpha \ll 1$ is easy as the scattered profile will be determined by $\Gamma_\alpha(x) \sim \exp(-x^2)$ and is Gaussian. The contribution from

the second term $Z\left(\frac{\alpha^2}{1+\alpha^2}\right)^2 \Gamma_\beta(y)$ will be negligible ($\alpha^4$ smaller).

For $\alpha \gtrsim 1$, $\Gamma_\alpha(x)$ has a maximum near $x = x_0$ where $x_0$ is the solution of the dispersion relatonship.

$$f(x_0) - 1 = \alpha^{-2} \qquad \text{(See Equation (38))} \qquad (41)$$

Very close to $x_0$, $\Gamma_\alpha(x)$ can be approximated by the Lorentzian shape because

$$\Gamma_\alpha(x) \simeq \frac{\exp(-x^2)}{[1+\alpha^2(1-f(x))]^2 + \pi\alpha^4 x^2 \exp(-2x^2)}$$

$$= \frac{\alpha^2 \exp(-x^2)}{\alpha^2[1-\alpha^2(f(x)-1)]^2 + \pi\alpha^4\alpha^2 x^2 \exp(-2x^2)}$$

Now for $x \gg 1$ we have the asymptotic expansion

$$f(x) - 1 \simeq (2x^2)^{-1}\left[1 + \frac{3}{2x^2} + \frac{15}{4x^4} + \cdots\right]$$

Using the first term as an approximation

$$f(x) - 1 \simeq \frac{1}{2x^2}$$

One can write $\Gamma_\alpha(x) = \dfrac{\frac{1}{2}\alpha^2 \exp(-x^2)}{\frac{1}{2}\alpha^2[1-\alpha^2/2x^2]^2 + \frac{1}{4}\pi\alpha^8 \exp(-2x^2)}$

Now

$$\tfrac{1}{2}\alpha^2\left[1 - \frac{\alpha^2}{2x^2}\right]^2 = \tfrac{1}{2}\alpha^2 \cdot \alpha^4[f(x_0) - f(x)]^2 = 4(x-x_0)^2$$

$$\therefore \quad \Gamma_\alpha(x) = \tfrac{1}{2}\alpha^2 \exp(-x^2)\left\{4(x-x_0)^2 + \tfrac{1}{4}\pi\alpha^8 \exp(-2x^2)\right\}^{-1}$$

$$= \tfrac{1}{2}\alpha^2 \exp(-x^2)\left\{4(x-x_0)^2 + [\tfrac{1}{2}\pi^{\frac{1}{2}}\alpha^4 \exp(-x^2)]^2\right\}^{-1}$$

is therefore Lorentzian near $x_0$.

From (41) and the first two terms of the asymptotic expansion of $f(x)$, we have

$$(2x_0^2)^{-1}[1 + 3/2x_0^2] = \alpha^{-2}$$

It is easily varied that

$$x_0^2 = \tfrac{1}{2}(\alpha^2 + 3)$$

i.e.

$$\omega_0^2 = \omega_{pe}^2 + 3kT_e k^2/m_e$$

which is the well-known dispersion longitudinal (electrostatic) plasma oscillation. The satellites occur at $\pm\,\omega_0 = \pm\left(\omega_{pe}^2 + \frac{3kT_e k^2}{m_e}\right)^{\frac{1}{2}}$

The shape of $\Gamma_\beta(y)$ for the special case of greatest interest $Z = T_I/T_e$, $\alpha \to \infty$ and therefore $\beta = 1$ is almost flat-top. The shape of $\Gamma_1(y)$ differs from the Gaussian for non-interacting ions

ions because electrostatic potentials of the electrons $\sim kT_e$ are set up by the requirement that the electrons follow the charge density of the (slow) ions.

If $ZT_e > T_I$ as well as $\alpha \gg 1$, we have $\beta = \left(\frac{ZT_e}{T_I}\right)^{\frac{1}{2}} > 1$ and we have the corresponding case of the ion satellites whose shape can be similarly shown to be Lorentzian and occurred similarly at

$$\pm\,\omega_0' = \left(\omega_{pI}^2/1+\alpha^2 \;+\; 3kT_I k^2/m_I\right)^{\frac{1}{2}}$$

D. Integrated Intensity Calculations

The integrated intensities of the two contributions from $\Gamma_\alpha(x)$ and $\Gamma_\beta(y)$ will now be calculated.

For $\alpha \gg 1$

$$\pi^{\frac{1}{2}} \int_{-\infty}^{\infty} \Gamma_\alpha(x)\,dx = \pi^{-\frac{1}{2}} \int_{-\infty}^{\infty} \frac{\frac{1}{2}\alpha^2 \exp(-x_0^2)}{4(x-x_0)^2 + \left[\frac{1}{2}\pi^{\frac{1}{2}}\alpha^4 \exp(-x_0^2)\right]^2}$$

$$= \pi^{-\frac{1}{2}}\,\tfrac{1}{2}\alpha^2 \exp(-x_0^2)\,\pi \,/\, \tfrac{1}{2}\pi^{\frac{1}{2}}\alpha^4 \exp(-x_0^2)$$

$$= \alpha^{-2} \qquad \text{(for both satellites)}$$

For general values of $\alpha$, the calculation is a little more complicated.

Now $\quad \Gamma_\alpha(x) = \dfrac{\exp(-x^2)}{\left[1+\alpha^2-\alpha^2 f(x)\right]^2 + \pi\alpha^4 x^2 \exp(-2x^2)}$

Where $\quad f(x) = 2x \exp(-x^2) \int_0^x \exp t^2\,dt$

Let $\quad G_e(x) = 1 - f(x) - i\,\pi^{\frac{1}{2}}\,x \exp(-x^2)$

$$\therefore\; \pi^{-\frac{1}{2}}\Gamma_\alpha(x) = \mathrm{Im}\left\{\frac{1}{\pi\alpha^2 x}\left[\frac{1}{1+\alpha^2 G_e(x)} - \frac{1}{1+\alpha^2}\right]\right\}$$

Let $\quad x = Re^{i\theta}$

$$\therefore\; \pi^{-\frac{1}{2}}\int_{-\infty}^{\infty}\Gamma_\alpha(x)\,dx = \lim_{R\to\infty}\frac{1}{\pi\alpha^2}\,\mathrm{Im}\int_0^{2\pi}\left[\frac{1}{1+\alpha^2 h(Re^{i\theta})} - \frac{1}{1+\alpha^2}\right] i\,d\theta$$

Now $\quad \lim_{R\to\infty} h(Re^{i\theta}) \longrightarrow 0$

$$\therefore\; \pi^{-\frac{1}{2}}\int_{-\infty}^{\infty}\Gamma_\alpha(x)\,dx = \frac{1}{1+\alpha^2} \qquad \text{(for both satellites)}$$

Similarly for $\quad Z = T_I/T_e = 1$

$$\left(\frac{\alpha^2}{1+\alpha^2}\right)^2 \pi^{-\frac{1}{2}}\int_{-\infty}^{\infty}\Gamma_\beta(y)\,dy = \frac{\alpha^4}{(1+2\alpha^2)(1+\alpha^2)}$$

So that the contribution $\Gamma_\beta(y)$ is larger than the contribution $\Gamma_\alpha(x)$ by a factor $\frac{\alpha^4}{1+\alpha^2}$. For large $\alpha$ this is approximately $\alpha^2/2$ and

hence the ratio of the central peak to each satellite is $\alpha^2$.

E. Fortran Program for Calculation of Scattered Spectrum.

```
      SUBROUTINE FLUCT(S,WAVE,ATWT,Z,TE,TI,THETA,ALF,ELDEN,DLAMB)
C  CALCULATION OF THE SPECTRAL DENSITY S/ELDEN
C     UNITS OF WAVE, DLAMB ARE CM
C     UNITS OF ELDEN       ARE CM**-3
C     UNITS OF TE, TI      ARE DEG K
C     UNITS OF THETA       ARE DEG
C     IF ELDEN IS SPECIFIED,THEN ALPHA IS CALCULATED
C     IF ELDEN IS PUT ZERO, THEN ALPHA IS READ IN
      REAL K
      PI = 3.14159265
      BT = 3.299E-12
C          MASS ELECTRON / 2 BOLTZ
      K= 4.*PI * SIN(THETA*PI/360.) / WAVE
      BETAE = SQRT(BT/TE)
      BETAI = SQRT(BT*1836.*ATWT/TI)
      DEBL = SQRT(TE/ELDEN) * 6.90
C                          SQRT(BOLTZ / 4 PI)/ELECTRON CHARGE
      IF (ELDEN.NE.0.0)  ALF = 1./(DEBL*K)
      AAE = ALF*ALF
      AAI = AAE*Z*TE/TI
      U = DLAMB * 2.*PI*2.998E10 / (WAVE*WAVE*K)
C     U IS OMEGA / K
      XE = BETAE * U
      XI = BETAI * U
      CALL G  (FE, PE, QE, XE, AAE)
      CALL G  (FI, PP, QI, XI, AAI)
      ZETA = BETAE*FE* ((1.-PP)*(1.-PP)+QI*QI) + Z*BETAI*FI*
     1 (PE*PE+QE*QE)
      EPS = (1.-PE-PP)*(1.-PE-PP) + (QE+QI)*(QE+QI)
      S = 3.54490*ZETA/(EPS*K)
C         2 SQRT(PI)
      RETURN
      END
```

(Continued on next page)

```
      SUBROUTINE G (F, P, Q, X, AA)
C     P IS THE REAL PART OF G, Q IS THE IMAGINARY PART
C     AA IS ALPHA SQUARED
C     F IS WITHOUT THE FACTOR BETA
      XX = X*X
      F = EXP(-XX)
      Q = 1.77245*X*F*AA
      SER = 1.0
      TERM = 1.0
      AN = 1.0
      IF (X.GE.3.0)  GO TO 28
C     ABSOLUTELY CONVERGENT SERIES
29    TERM = - TERM * 2.*XX/AN
      SER = SER + TERM
      AN = AN + 2.
      IF (ABS(TERM).GT.1.E-4)   GO TO 29
      P = -SER*AA
      RETURN
28    SER = 0.0
C     ASYMPTOTIC SERIES
27    TERM = TERM * AN * 0.5 / XX
      IF (AN*.5.GT.XX)   GO TO 26
      SER = SER + TERM
      AN = AN + 2.
      IF (ABS(TERM).GT.1.E-4)  GO TO 27
26    P = SER*AA
      RETURN
      END
```

## REFERENCES


1. E.E.Salpeter, Phys. Rev.120, 1528(1960).

2. J.A.Fejer, Can.J.Phys. 38,1114(1960).

3. J.P.Dougherty and D.T.Farley,Pro.Roy.Soc.(London) A259,79(1960).

4. M.N,Rosenbluth & N.Rostoker,Phys. Fluids 5, 776(1962).

5. K.L.Bowles, Phys. Rev.Letters 1, 12(1958).

6. F.W.Perkins,E.E.Salpeter,K.O.Yngnessen,Phys.Rev.Letters 14, 15(1965).
7. R.A.Stern & M.Tzoar, Phys.Rev.Letters 15, 485(1965).

8. G.Fiocco and E.Thompson,Phys.Rev.Letters 10, 89(1963).

9. E.Funfer,B.Kronast,H.J.kunze,Phys.Letters 5,125(1963).

10. H.J.Kunze,E.Funfer,B.Kronast,W.H.Kegel,Phys.Letters 11, 42(1964).
11. W.E.R.Davies and S.A.Ramsden, Phys.Letters 8,179(1964).

12. U.Ascoli-Bartoli,J.Katzenstein and L.Lovisetto, Nature 204, 672(1964).
13. A.W.De Silva,D.E.Evans and M.J.Forrest,Nature 203,1321(1964).

14. S.A.Ramsden,W.E.R.Davies,paper presented in the meeting of the American Physical Society(1964).
15. S.A.Ramsden,W.E.R.Davies,Phys.Rev.Letters 16,303(1966).

16. P.W.Chan & R.A.Nodwell,Phys.Rev.Letters 16, 122(1966).

17. see for example:J.M.Stone, Radiation and Optics (Mcgraw Hill, 1963).
18. L.Spitzer,Physics of Fully Ionised Gases (Interscience,1956).

19. see for example:L.D.Landau & E.M.Lifshitz, The Classical Theory of Fields (Addison Wesley,1958).
20. see for example:H.G.Griem, Plasma Spectroscopy(Mcgraw Hill, 1964).
21. A.van der Ziel, Noise ( Prentice-Hall Inc.,1954).

22. Lord Rayleigh, Phil. Mag. 47,375(1899).

23. G.A.Theophanis, Rev.Sci.Inst. 31, 427(1960).

24. F.L.Curzon and P.R.Smy,Rev.Sci.Inst. 32,756(1961).

25. B.Ahlborn,Z.Naturforsch. 20,466(1965).

26. IPP Report,Institute fur Plasmaphysik,Garching Bei Munchen (1963).
27. Nyugen-Quang-Dong, Phys.Letters 21, 159(1966).

28. see for example:S.Gartenhaus,Elements of Plasma Physics, (Holt, Rinehart and Winston,1964).